Projected changes in Oregon precipitation due to anthropogenic climate change

David W. Pierce

Daniel R. Cayan

Division of Climate, Atmospheric Sciences, and Physical Oceanography
Scripps Institution of Oceanography
University of California San Diego

2024-11-20 version 1

DOI: 10.13140/RG.2.2.15737.48489

Introduction

Precipitation in the state of Oregon will be altered in the future due to anthropogenic climate change, which is the process where human activity modifies the climate on both the global and local scale. The single largest global driver of anthropogenic climate change is the release of greenhouse gases into the atmosphere, particularly carbon dioxide through the combustion of fossil fuels. Other gases such as methane and some byproducts of industrial processes have important contributions as well. Greenhouse gases warm the planet by reducing the ability of longwave radiation to cool the surface of the Earth by escaping to space, a process that has been understood for over a century (Arrhenius, 1896). Additional human activities influence the climate as well, such as the release of aerosols, primarily from burning coal, and land use changes, principally deforestation and agriculture (IPCC, 2023).

The purpose of this work is to document future projected changes in precipitation across the Pacific Northwest, with a focus on Oregon, that arise from anthropogenic climate change scenarios. The fundamental data underpinning these projections are results from the latest set of global climate models that are part of the Climate Model Intercomparison Project, version 6 (CMIP6; Eyring et al., 2016). The CMIP6 global climate models are produced and run by different groups of climate scientists all around the world and represent the best estimations we currently possess of how future climate change will play out on global to continental scales.

The CMIP6 global climate models are run under a variety of scenarios of future greenhouse gas emissions, aerosol emissions, land use changes, and population, technological, and economic growth; these scenarios are termed shared socioeconomic pathways (SSPs) (O'Neill et al. 2014,

2016; Riahi et al. 2017). We considered three SSPs: 2-4.5, 3-7.0, and 5-8.5. SSP 2-4.5 assumes moderate reductions in emissions, continuation of historical social and economic trends, and moderate challenges to mitigation and adaptation. SSP 3-7.0 assumes a doubling of carbon dioxide emissions by 2100, conflicts among regions, and substantial challenges to mitigation and adaptation. SSP 5-8.5 assumes that carbon dioxide emissions double by 2050 with substantial challenges to mitigation, but minor challenges to adaptation (O'Neill et al. 2016). We analyzed precipitation during four periods: historical (1950-2014), early twenty-first century (2015-2044), mid-twenty-first century (2045-2074), and late twenty-first century (2075-2100).

The CMIP6 global climate models have a relatively coarse spatial resolution, typically in the range of 70 to 200 km depending on the model. This renders them unable to resolve Oregon's complicated topography. Features such as the Coast Range, Willamette Valley, and Cascades are poorly represented by global climate models, but have an important role in determining the local climate. For this reason we do not use the global climate model data directly, but rather employ a version of the global climate model data statistically downscaled to a 1/16th degree latitude-longitude grid (nominally 6 km) by the LOCA2 method (Pierce et al. 2014; Pierce et al. 2015; Pierce et al. 2023). The LOCA2 data set covers the period 1950-2100, and the CMIP6 historical period ends in 2014. Together these determine the historical period we use here, 1950-2014.

The LOCA2 statistical downscaling method uses historically observed relationships between weather and climate on the large (50-1000 km) and small (6 km) scale to regionalize the global climate model results to a particular location, in this case the Pacific Northwest. Downscaling adds the effects of local topography to the original global climate model results, a necessary requirement in regions with complex terrain. LOCA2 precipitation was trained on the station-based observational data set of Pierce et al. 2021; this data set is referred to as the observations below.

The impacts of climate change on ecosystems, society, and the economy are felt primarily at the extremes. We therefore emphasize analysis of the predicted changes in extreme precipitation, although we begin with a brief overview of changes in mean precipitation and frequency of wet days for context. Additionally, regional water resources are critically dependent on whether winter precipitation in the Pacific Northwest falls as rain or snow. Hence, we also investigate the temperature at which precipitation will fall in the future and analyze future snowfall rates constructed from precipitation combined with daily minimum and maximum temperatures.

Model selection

Although the full LOCA2 archive includes 27 global climate models, not all are equally skilled at reproducing observed weather and climate over the western U.S. In this work we follow the guidance of Krantz et al. 2021, who evaluated available data from approximately 30 CMIP6 global climate models on their ability to realistically capture both important weather processes that affect the west coast of the U.S. and realistic surface mean annual and seasonal climate and variability over the greater California region, including western Nevada and southern Oregon. Although this region does not directly include northern Oregon, many of the weather processes that determine the climate of Oregon are the same as those that affect Northern California. Additionally, our previous evaluations of global climate models for regional climate change studies shows that the main objective in selecting global climate models is to eliminate the worst performing models,

which are consistently poor performers across a wide variety of metrics and regions. By contrast, the best performing models have different sets of tradeoffs in the various performance metrics.

The process-based metrics included measures of Northern Hemisphere blocking (high pressure systems that block the west-to-east movement of mid-latitude weather systems), offshore wind shear, the El Niño-Southern Oscillation, and vertically integrated column water vapor, sea level pressure, and zonal wind on days of extreme precipitation. The surface climate and variability metrics included seasonal means of temperature and precipitation, the standard deviation of temperature and precipitation averaged into 1-, 5-, and 10-year blocks, the amplitude and phase of the annual harmonic of temperature and precipitation (used to evaluate the seasonal cycle), and the standard deviation of monthly values of temperature and precipitation in January and July, used to evaluate variability on shorter timescales than the seasonal means and variability. More details on the metrics and methodology to evaluate the metrics can be found in Krantz et al. 2021.

Table 1. Global climate models used in this work, their originating institutions, and the number of ensemble members available for each model for the SSP 2-4.5, 3-7.0, and 5-8.5 emissions scenarios, respectively.

Model	Institution	# ensemble members for SSP 2-4.5, 3-7.0, 5-8.5
ACCESS-CM2	The Commonwealth Scientific and Industrial Research Organisation (CSIRO), Australia	3, 3, 3
CEMS2-LENS	National Center for Atmospheric Research, Boulder, CO, USA	0, 10, 0
CNRM-ESM2-1	Centre National de Recherches Meteorologiques, France	1, 1, 1
EC-Earth3-Veg	European consortium of national meteorological services and research institutes, European Union	5, 4, 4
FGOALS-g3	Chinese Academy of Sciences, Beijing, China	3, 4, 3
GFDL-ESM4	Geophysical Fluid Dynamics Laboratory, Princeton, NJ, USA	1, 1, 1
IPSL-CM6A-LR	Institut Pierre-Simon Laplace, France	5, 10, 4
MIROC6	Division of Climate System Research, Atmosphere and Ocean Research Institute, The University of Tokyo, Japan	3, 3, 5
MPI-ESM1-2-HR	Max Planck Institute for Meteorology, Hamburg, Germany	2, 10, 2
MRI-ESM2-0	Meteorological Research Institute, Tsukuba, Ibaraki, Japan	1, 5, 1
TaiESM1	Research Center for Environmental Changes, Academia Sinica, Nankang, Taipei, Taiwan	1, 1, 0

The final selection of 11 global climate models is shown in Table 1. Although based primarily on the evaluation results in Krantz et al. 2021, some adjustment was made to avoid selecting two well performing models that were closely related, EC-Earth3 and EC-Earth3-Veg. Only EC-Earth3-Veg

was used in order to avoid over-representing the results from one particular model's physics. The models selected here are in general agreement, although not identical, with global models ranked according to an alternate evaluation aimed at Pacific Northwest hydroclimate applications by Lybarger et al. 2024. with 8 of the selected 11 global climate models falling into the upper half of the Lybarger model performance rankings.

Many of the models have multiple ensemble members, as noted in the third column of Table 1, which can be used to examine the effects of natural internal climate variability. Since natural climate variability is not the focus of this work, here we primarily evaluate the multi-model ensemble average (MMEA) of the models and ensemble members, since this gives a better representation of climate processes than any single global climate model alone (e.g., Pierce et al. 2009). To form the multi-model ensemble average we first average across all ensemble members for each individual model, then average the result across all models. Any determination of extremes or high order statistics is performed on individual model runs before they are aggregated across runs in order to avoid dilution by the averaging process. Constructing the multi-model ensemble average in this way avoids over-representation of models that have many ensemble members, since the number of ensemble members a model has is determined more by available computer resource budgets than by model quality.

Regional averaging

Some of our results are presented as regional averages. In this work we use the U.S. level 3 ecoregions (Omernik 1987) that fall in Oregon (Figure 1). Ecoregions are areas in which abiotic and biotic environmental attributes, such as climate, hydrology, vegetation, and land use, generally are similar. They are intended to provide a basis for research and management that is ecologically meaningful, particularly in contrast to political boundaries.

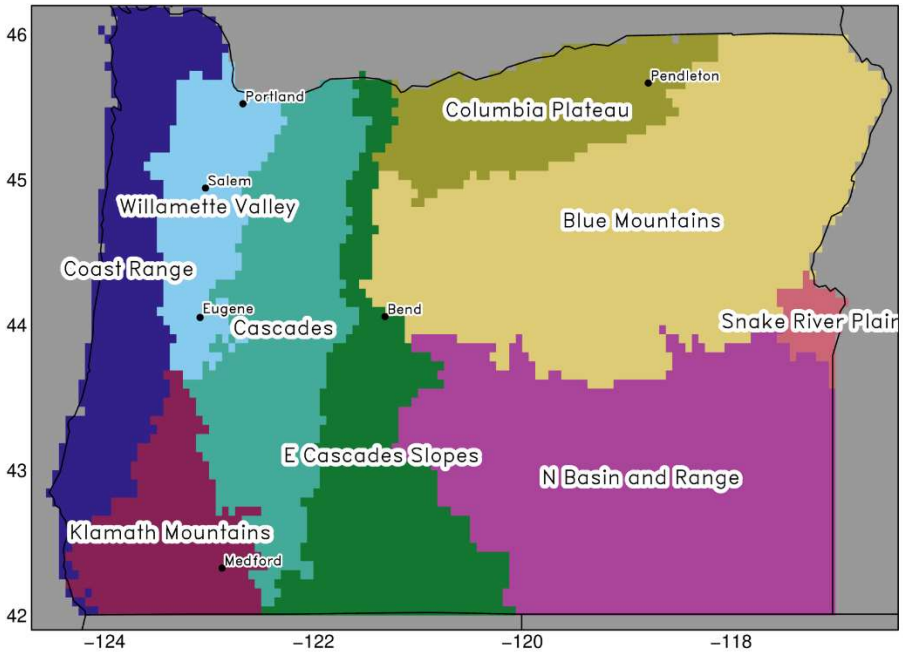

Figure 1. Level 3 U.S. ecoregions that fall in the state of Oregon, on the 6 km grid LOCA2 grid used here.

Mean precipitation changes

Although projected changes in mean precipitation are not our primary focus, they provide context for the later analysis of extremes and rain/snow split. The multi-model ensemble averaged mean precipitation over the historical period is shown in Figure 2 as a function of season: winter (Dec-Jan-Feb, or DJF), spring (Mar-Apr-May, or MAM), summer (Jun-Jul-Aug, or JJA), and autumn (Sep-Oct-Nov, or SON). The precipitation climatology of Oregon is characterized by wet winters and dry summers, with notable regional variability. The Coast Range and Cascades receive much more precipitation than eastern Oregon (especially in the southeast). Annual precipitation in the highly populated Willamette Valley was intermediate between the wet coastal areas and Cascade Range and the dry interior.

The multi-model ensemble average projected change in mean precipitation is shown in Figure 3 for the middle of this century (2045-2074) and the middle emissions scenario examined here (SSP 3-7.0). Additional figures are also available for all three time periods and three SSPs used in this work.

As shown in the top left panel of Figure 3, changes in annual mean precipitation are modest, in the range of 0-10% wetter conditions. However, the seasonal structure of the changes shows notable summer drying (bottom center panel), with decreased precipitation of 15% to 20% along much of Oregon's coast and the Columbia River gorge. These changes could have serious implications for ecosystems and wildfire incidence in the state. The projected precipitation changes at other periods in the 21st century and across SSPs, not shown here, confirm that the summer drying pattern seen in Figure 3 is a consistent feature of the model projections. The summer drying signal strengthens over time and with stronger anthropogenic climate forcing (higher SSPs).

The mean historical fraction of wet days (days when precipitation >= 0.5 mm/day) and projected change in mean fraction of wet days (%) are shown, annually and by season, in Figure 4. In winter the fraction of wet days exceeds 65% in the coastal regions of the Pacific Northwest and in the Cascades. Values drop to less than 15% in the summer over much of Oregon, especially east of the Cascade Range and in the Columbia Plateau. Model projected changes show a weak (0-6%) reduction in wet days in summer, with little change in the other seasons. The pattern of projected summer drying from Figure 3 roughly coincides with the pattern of reduction in summer fraction of wet days in Figure 4, although the greatest reduction in wet days is projected to be in the central and eastern Washington, while the greatest reductions in precipitation are in the Olympic peninsula. This, in addition to the projected reductions in precipitation being stronger than the reductions in fraction of wet days, suggests that the projected reductions in mean summer precipitation do not arise exclusively from fewer precipitating days.

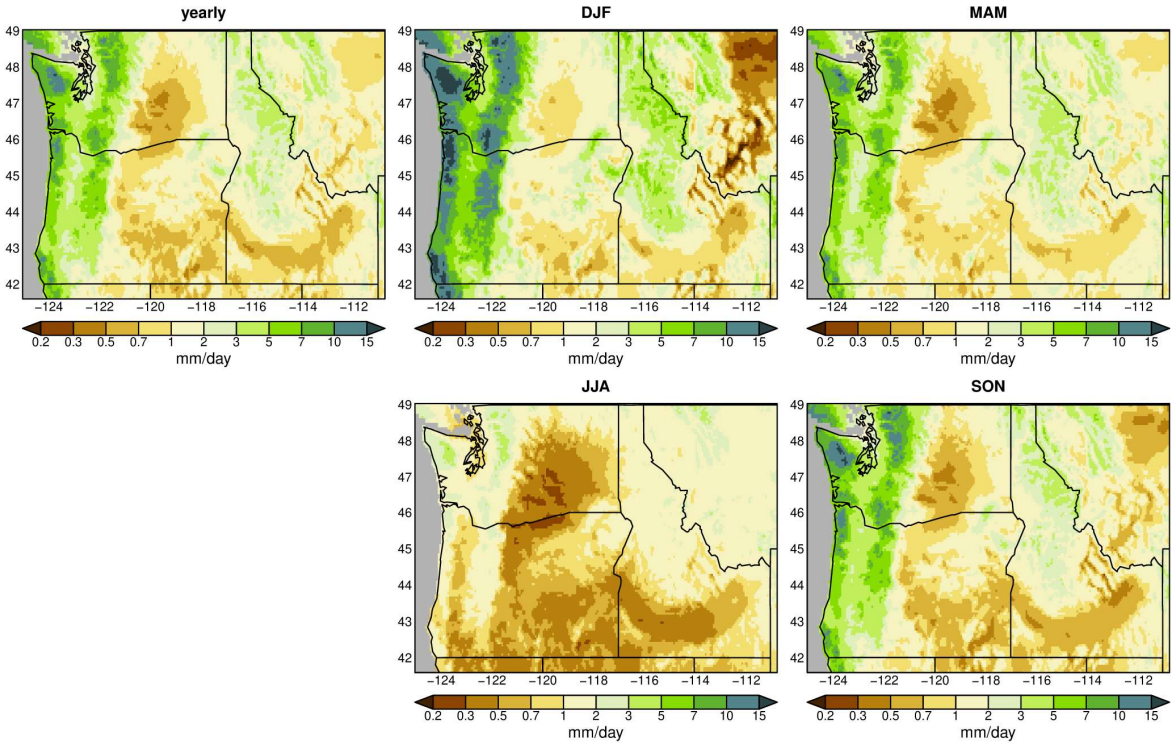

Figure 2. Multi-model ensemble average precipitation over the historical period (1950-2014), in mm/day. The top left panel shows the result for yearly averaged precipitation. The other panels show winter (Dec-Jan-Feb, or DJF), spring (Mar-Apr-May, or MAM), summer (Jun-Jul-Aug, or JJA), and autumn (Sep-Oct-Nov, or SON), as indicated in the panel title.

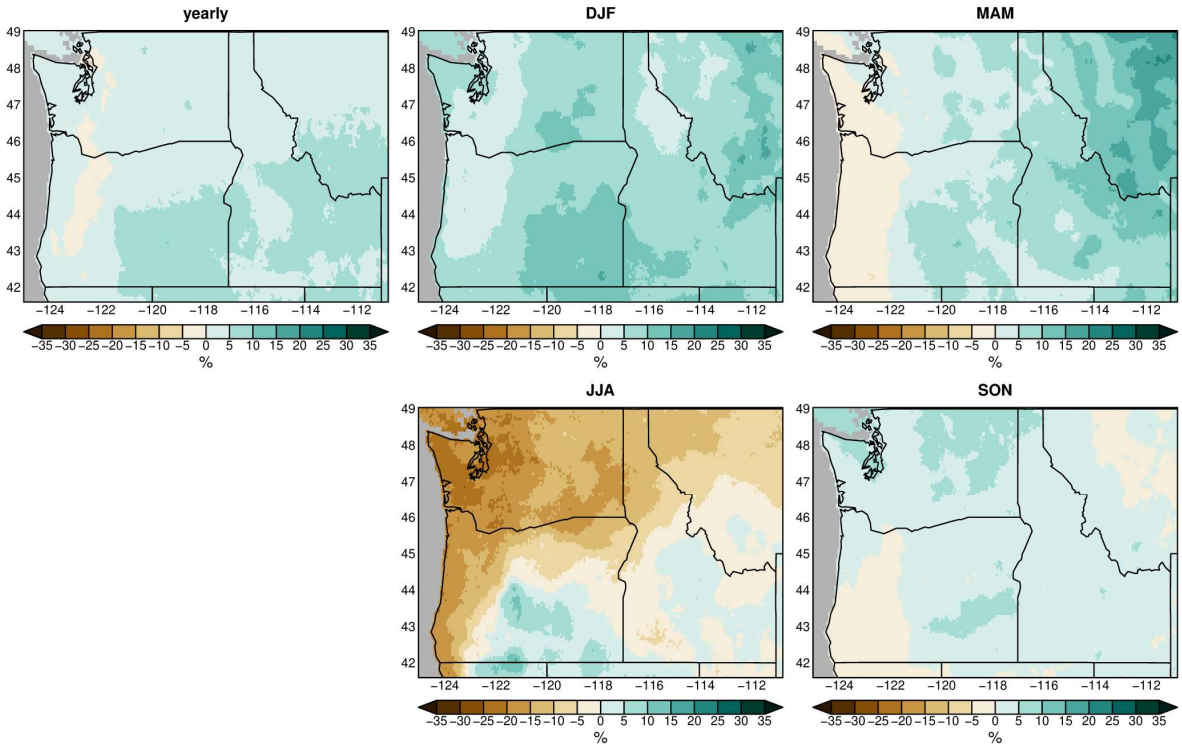

Figure 3. The multi-model ensemble average projected change in precipitation (%) for midcentury (2045-2074), for the medium emissions scenario considered in this work (SSP 3-7.0).

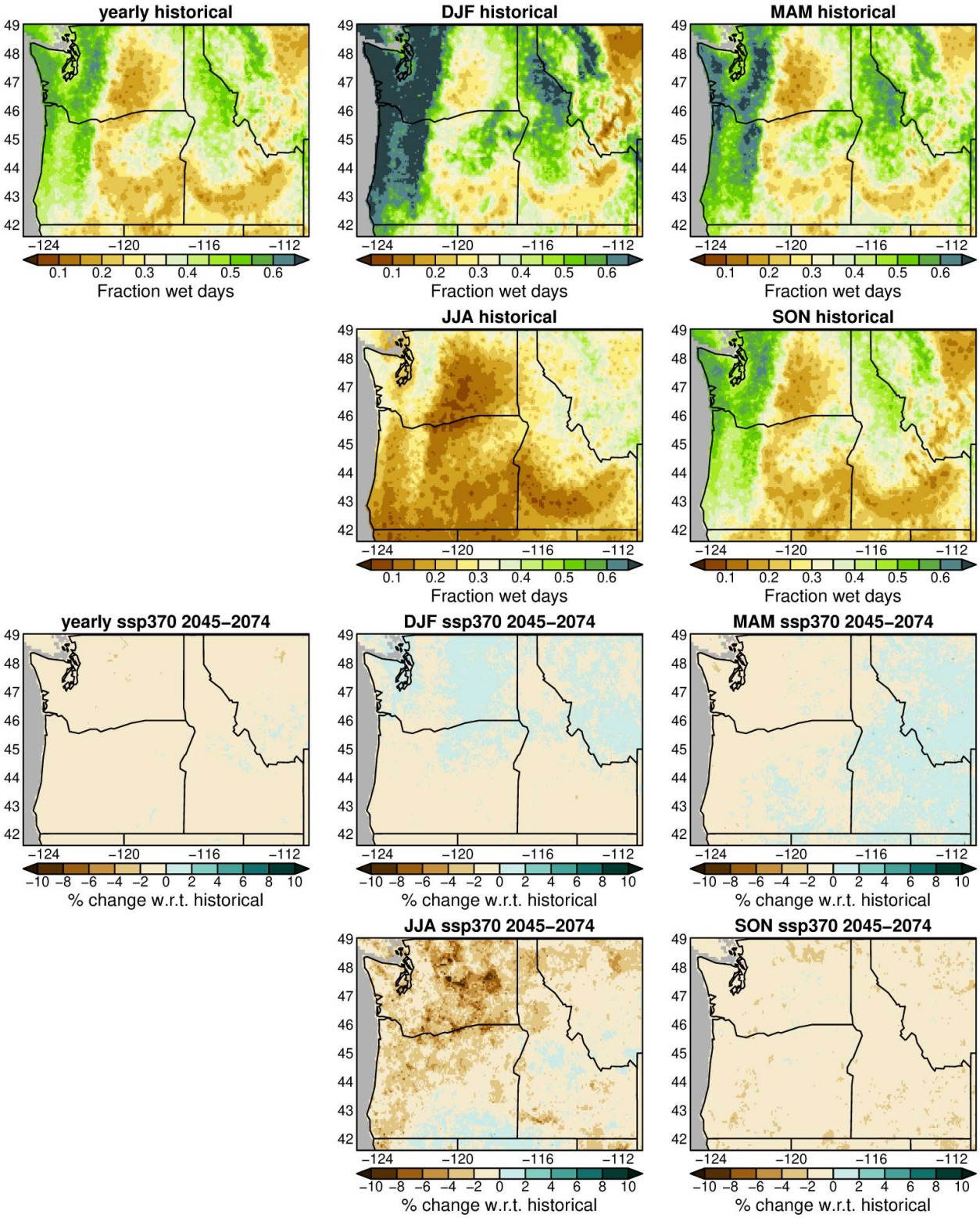

Figure 4. Upper set of panels: multi-model ensemble average fraction of wet days (precipitation >= 0.5 mm/day) over the historical period, yearly and by the indicated season. Lower set of panels: multi-model ensemble average projected change (%) in fraction of wet days, yearly and by the indicated season, for the SSP 3-7.0 emissions scenario by midcentury (2045-2074).

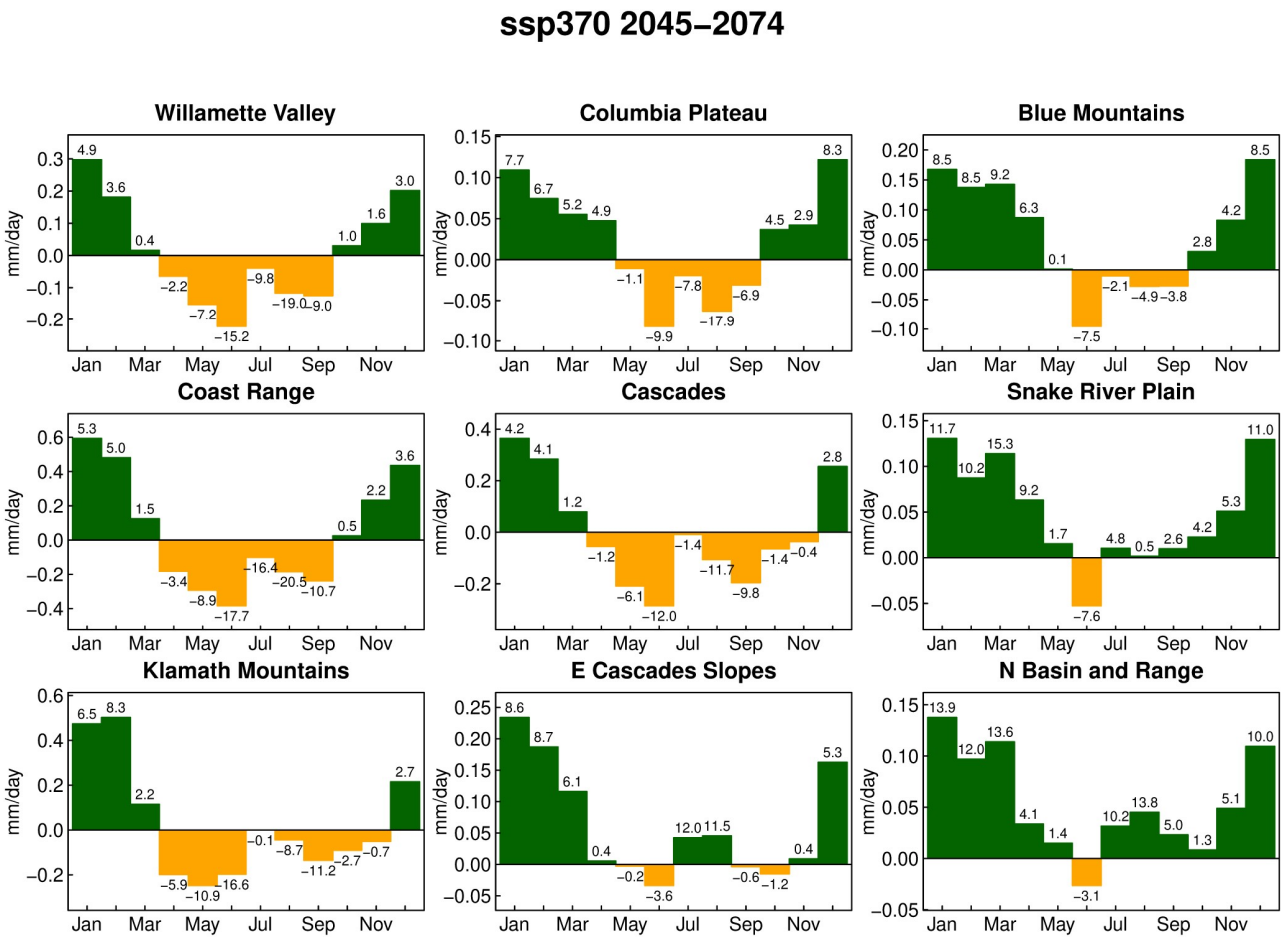

Figure 5. Multi-model ensemble average projected changes in monthly mean regional precipitation (mm/day) for midcentury (2045-2074), for the medium emissions scenario considered in this work (SSP 3-7.0). The numbers on the bars show the corresponding changes in percent.

Although the seasons used in Figures 2-4 are traditionally employed in meteorological analysis, seasonal averages do not capture all aspects of the projected monthly changes. Figure 5 shows the monthly mean changes projected by midcentury for the SSP 3-7.0 scenario. Each panel represents values averaged over one of the ecoregions present in Oregon (Figure 1), with the panels arranged in roughly geographical order. Many regions have negative projected changes in September but positive changes in November, splitting the Sep-Oct-Nov autumn period used here, including the Willamette Valley, Columbia Plateau, Blue Mountains, and Coast Range. In general, the drying in the western/northwestern part of the state extends from April through September, and even into November in the Klamath Mountains and Cascades ecoregions.

Projected extreme precipitation changes

Figure 6 shows historically observed estimates of wet day (>= 0.5 mm/day) precipitation at the 95th, 99th, and 99.9th percentile, by season and annually. The highest values are seen in autumn (SON)

and winter (DJF), and the lowest values in spring (MAM) and summer (JJA). Geographically, the highest values are seen in the Olympic peninsula and southern Oregon along the Pacific Coast.

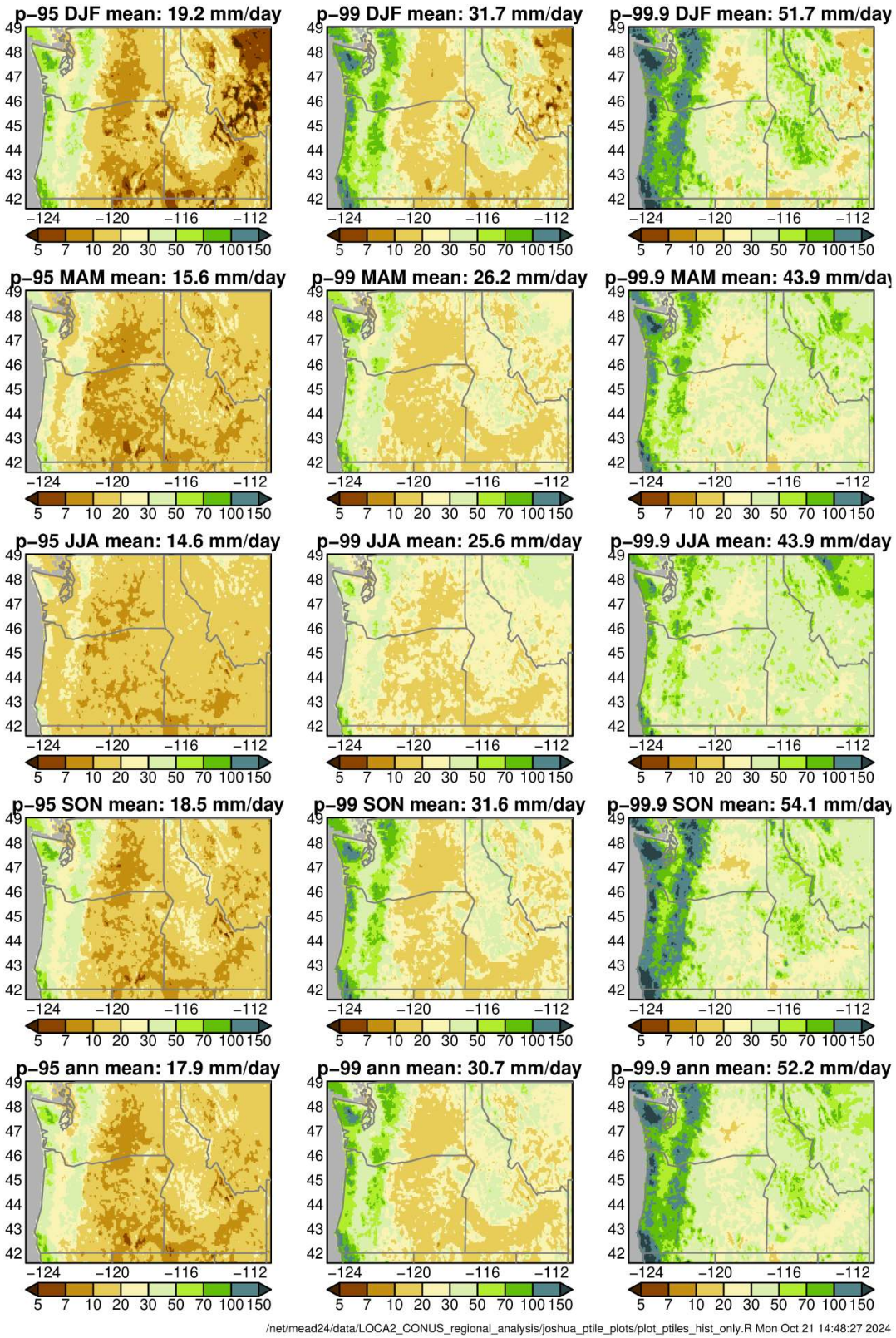

Figure 6. Historically observed percentiles of wet (>0.5 mm/day) day precipitation over the period 1950-2014, by season and annually (rows) and for the 95th, 99th, and 99.9th percentiles (columns). The title shows the mean over the entire domain.

Our main focus in this work is on projected future changes in extreme precipitation. Figure 7 shows the multi-model ensemble average-projected future changes in extreme wet day precipitation at the 99th percentile value, using annual data, for all time periods and SSPs examined here. Changes are nearly all positive for all three SSPs and all three percentiles, ranging from a few percent to more than 20 percent wetter.

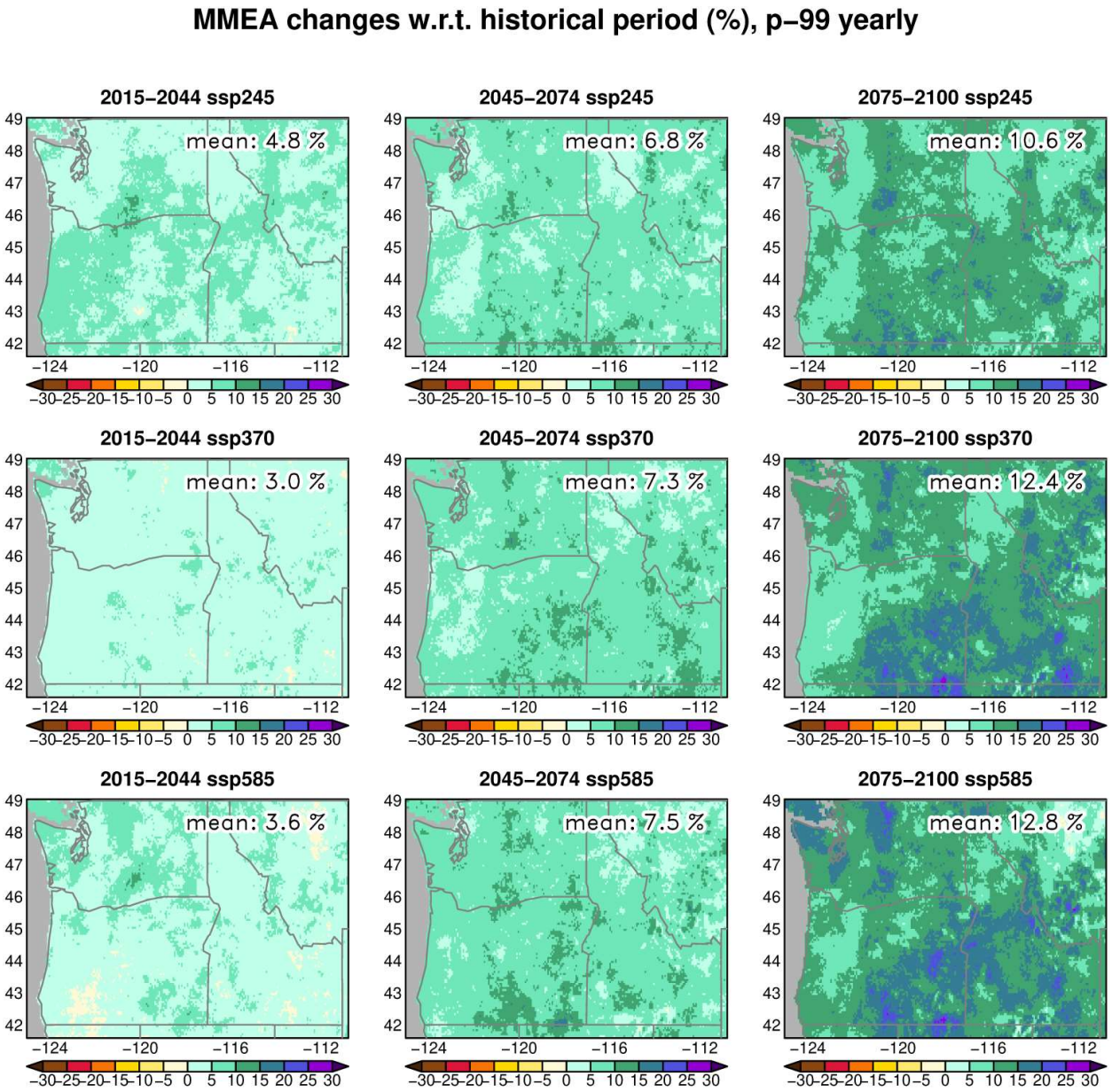

Figure 7. Multi-model ensemble average projected change in precipitation (%) at the 99th percentile of wet days, for different periods in the century (columns) and SSPs (rows). The mean over the entire domain is also shown in each panel.

For midcentury (2045-2074) and beyond, all projected changes in multi-model ensemble average extreme precipitation calculated annually are increases. This is in accordance with the general thermodynamic expectations of anthropogenic climate change, since warmer air temperatures will lead to an increase in the saturation vapor pressure of water vapor in the atmosphere, yielding an increase in the amount of water available to precipitate onto the landscape (e.g., Westra et al. 2014; Kroner et al. 2017; Norris et al. 2019; Harp and Horton, 2022). For the middle of this century under SSP 3-7.0 (medium) forcing, the average increase over the Pacific Northwest is about 7.3%. For all three SSPs, the projected increase in extreme precipitation grows in time throughout the 21st century.

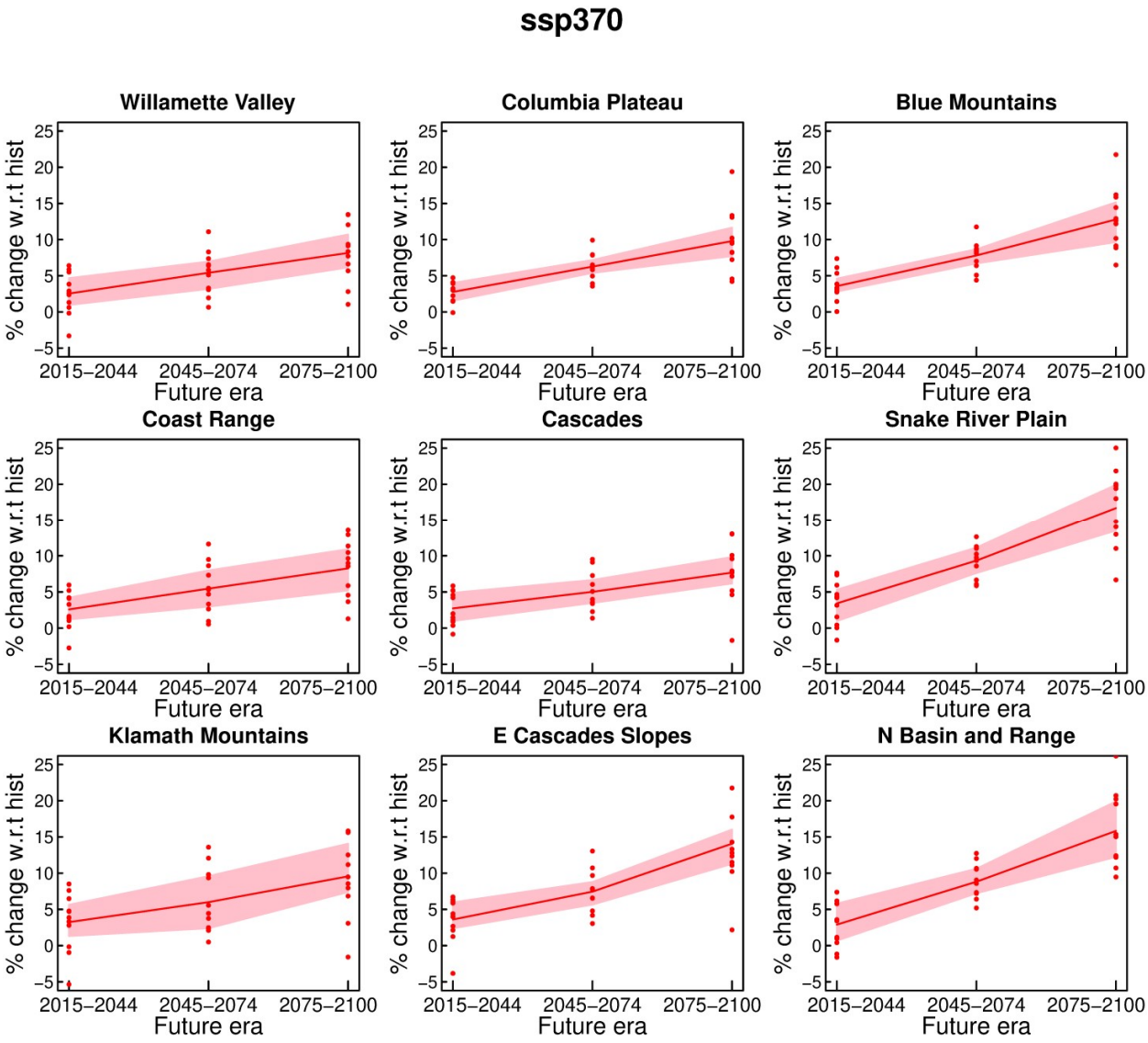

Figure 8. Projected change in precipitation (%) at the 99th percentile of wet days across the entire year, by region, as a function of time for the SSP 3-7.0 emissions scenario. The red line is the multi-model ensemble average. The pink envelope shows the interquartile range (IQR) across all 11 available models. Red dots show the results from each individual model.

The multi-model ensemble average has the advantage that it provides a better representation of climate processes than any individual model, but model variability can be better understood by examining the range of projected changes across the available models. Figure 8 shows the range in the projected change of 99th percentile wet-day precipitation for the entire year across all 11 models that are available for the SSP 3-7.0 emissions scenario. Early in the century individual models can show negative changes even though the overall multi-model ensemble average and interquartile range (IQR; pink region) are positive, and the multi-model ensemble average grows as the century progresses. On the other hand, some models show extreme precipitation increases that are substantially higher than those seen in the multi-model ensemble average. The future precipitation extremes seen in any one particular location, such as Salem, Eugene, or Bend, will be a combination of two factors: 1) forced changes from anthropogenic climate change that cause a systematic tendency towards increased precipitation extremes for known physical reasons (primarily increasing water vapor in the atmosphere as temperatures warm); and 2) natural weather and climate variability of the kind that is experienced every year: some winters are wetter than others, sometimes heavy storms pass north or south of a city, etc. These issues of variability and uncertainty are discussed more below.

Similar to projected changes in mean precipitation (Figure 3), projected changes in the 99th percentile of wet day precipitation by mid-century under SSP 3-7.0 (the middle emissions scenario considered here) also show a distinct seasonal cycle with the lowest values in summer (Figure 9). Averaged across the entire Pacific Northwest domain, there is a 9.0% increase in winter (DJF) and an 8.8% increase in autumn (SON). The state of Oregon follows this larger regional pattern, with the largest projected increases in winter and second largest in autumn. In both the Pacific Northwest and state of Oregon, projected summer changes are weak, just over a percent when averaged over the domain. The lowest values (weakly negative) are seen in coastal Oregon, especially in the south.

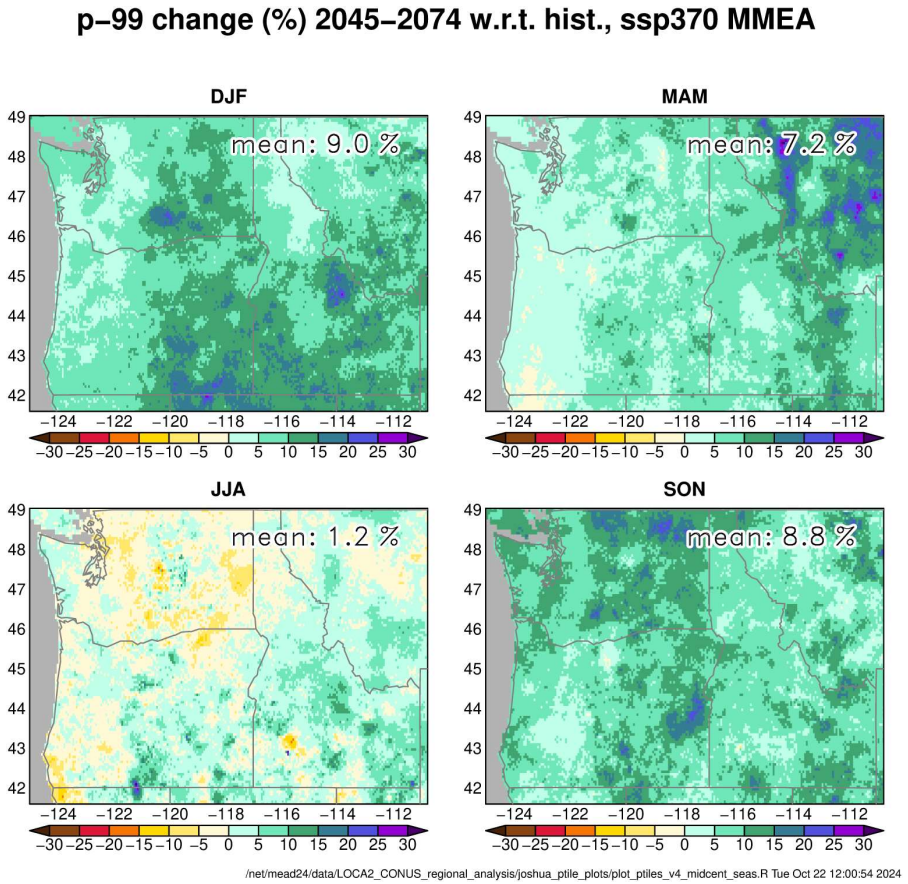

Figure 9. Multi-model ensemble average change in precipitation (%) at the 99th percentile of wet days, for different seasons as indicated in the panel titles. Values are shown for mid-century (2045-2074) under the SSP 3-7.0 emissions scenario.

As the century progresses, the magnitude of 99th percentile wet day precipitation continues to increase in winter, spring, and autumn (Figure 10, showing the period 2075-2100), especially in winter in Southeastern Oregon. Summer changes remain modest, by contrast.

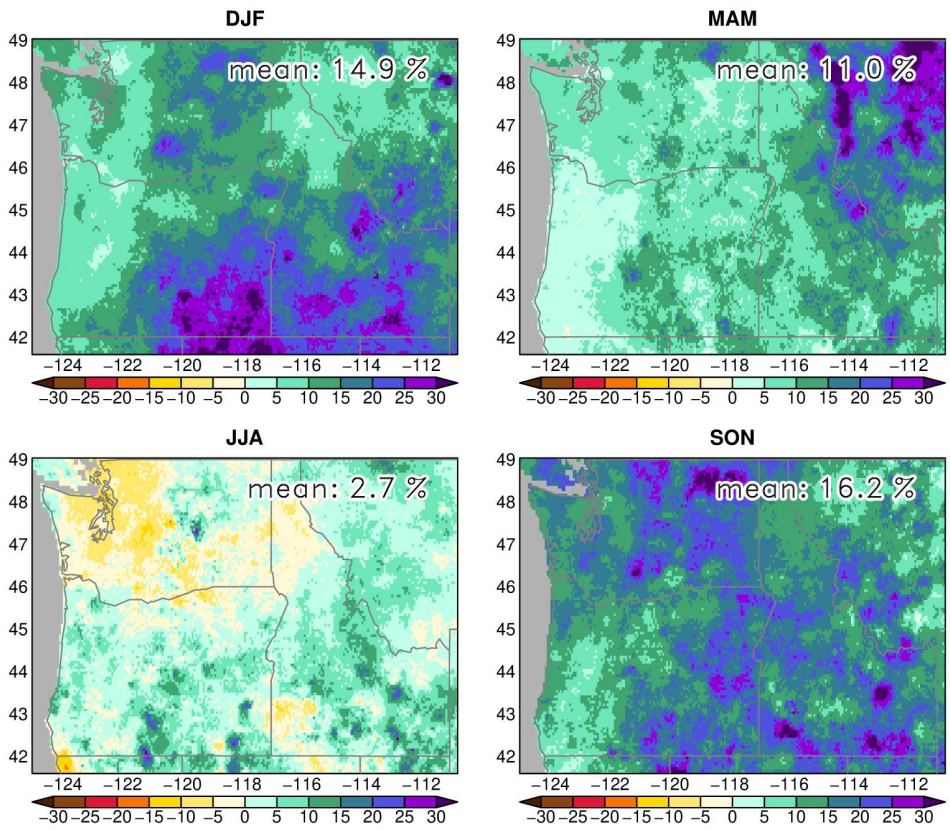

Figure 10. Same as Figure 9, but for the end of this century (2075-2100).

Figure 11 illustrates how the projected precipitation changes vary by season and by percentile. In each panel, results are shown for the 90th, 95th, 99th, and 99.9th percentiles (along the X axis), and for winter (DJF), spring (MAM), summer (JJA), and autumn (SON) (colored lines). Setting aside summer for the moment, most regions exhibit a general tendency for extreme values to increase most at the highest extremes (99.9th percentile). The largest increases are found in autumn and winter, with autumn increases tending to be the largest in the more northwesterly part of Oregon and winter increases dominating in the southeastern part of the state. Summer changes are more variable, although the western and Northwestern parts of the state tend to have a consistent pattern of reduced extremes at the 90th percentile that become progressively less reduced at the higher percentile levels. In the southeastern part of the state, summer changes are overall modest and there is a tendency to find decreasing extremes at the highest percentile values.

Overall, despite the complexity of responses across the state, one high level takeaway is that there is some cause for concern given the consistently projected increases in extreme precipitation at the very highest values in the more populated regions of the state, especially the Willamette valley. This is particularly so since the greatest increases are seen in autumn and winter, which are already the wettest seasons in that region. Such increases, which can approach 20% in autumn, could prove a strain to local infrastructure designed to address flooding risks.

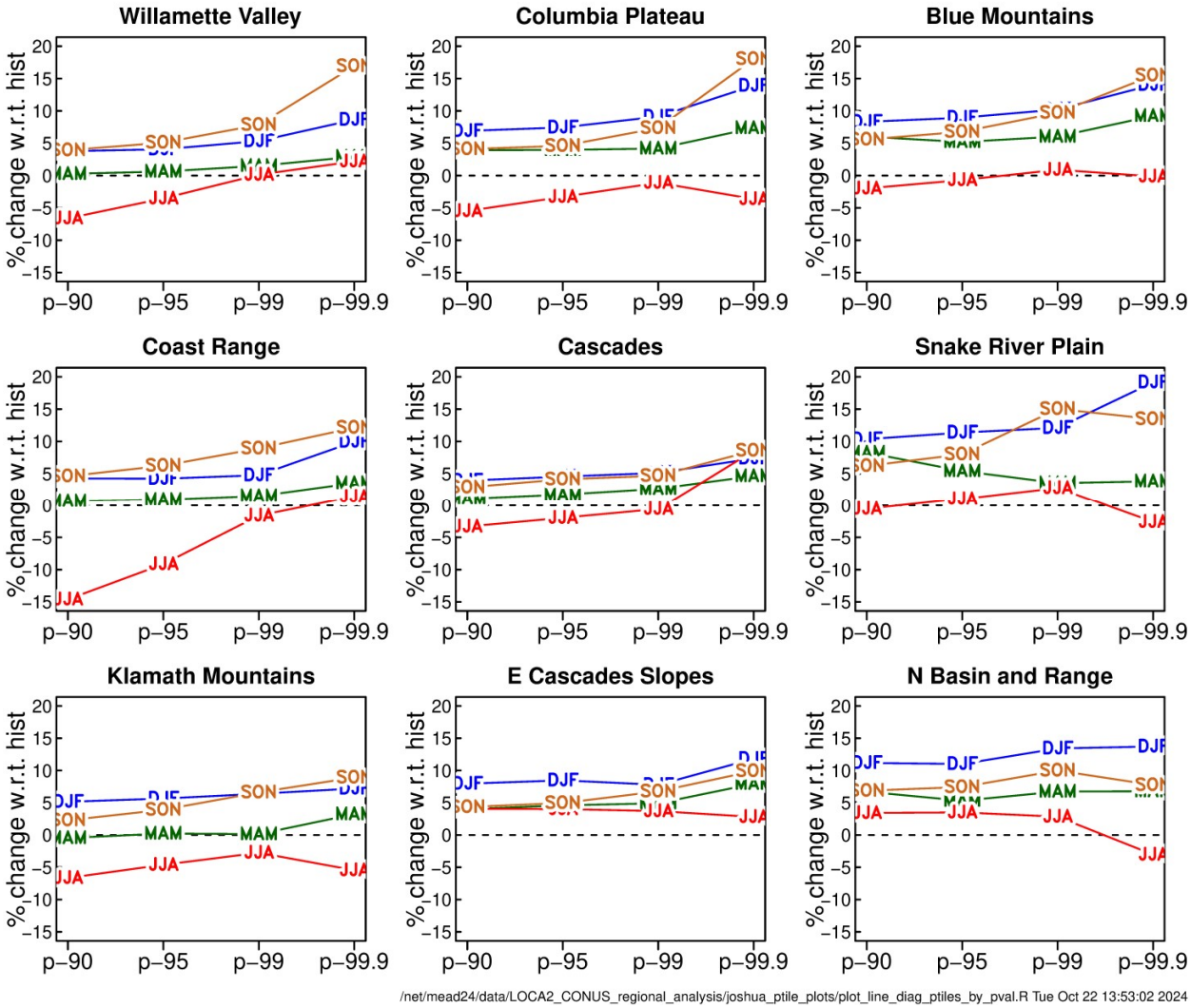

Figure 11. Multi-model ensemble average projected changes (%) in extreme precipitation as a function of percentile of wet day precipitation (X axis; from the 90th to the 99.9th percentile), season (as indicated by the color lines), and region (by panel, arranged roughly geographically in the state). Results are shown for mid-century (2045-2074) using scenario SSP 3-7.0.

Precipitation values at even higher extremes can be examined by looking at the return values of daily precipitation over return periods of a decade to a century. For instance, if, on average, the daily maximum precipitation in a 10 year period is 250 mm, then the return period is 10 years and the return value is 250 mm. Return values also can be interpreted as probabilities: a 10-year return value has a 10 percent probability of occurrence in a given year, while a 50-year return value has a 2 percent probability of occurrence in a given year. We estimate return values using annual block maxima and the method of L-moments (Hosking, 1990), which is well suited to this application since it is a robust estimator and relatively quick to compute, advantages when applying it across numerous global climate models.

The return values of wet-day precipitation estimated from observations are shown in Figure 12 for return periods of 10, 20, 50, and 100 years. Once in a century return values of daily precipitation

reach about 100 mm in the Willamette Valley, and over 350 mm on the Olympic peninsula and parts of the southeastern coast of Oregon.

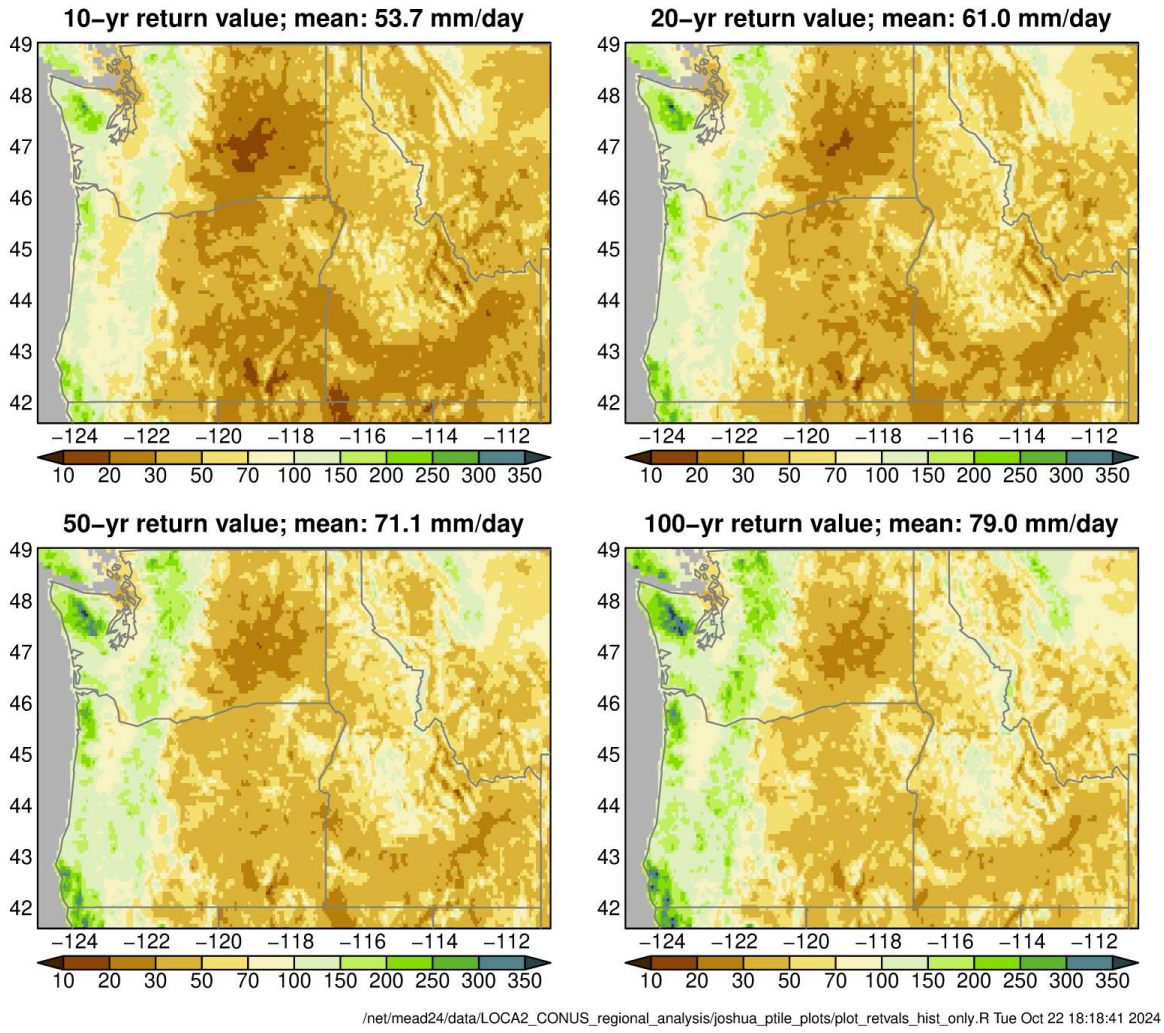

Figure 12. Return values (mm/day) of daily wet-day precipitation from the observations over the historical period (1950-2014). The title shows the mean value over the entire domain.

The multi-model ensemble average projected change in return values ranging from the wettest day in a decade to the wettest day in a century are shown in Figure 13, by region, for the SSP 3-7.0 emissions scenario. Results are shown for early century (2014-2044, blue “E”), midcentury (2045-2074, brown “M”) and late century (2075-2100, red “L”).

All regions in Oregon show increases in projected future extreme return values. Mid-century increases range from 11% to 20% for the wettest day in a century (100-yr return value). Generally speaking, increases become larger as the century progresses from Early to Mid to Late, with the exception of the Willamette Valley and Columbia Plateau regions, where late century projected changes are little different from midcentury projected changes. In other parts of the state late century changes become quite substantial, with 100-yr return values commonly more than 20% larger than historical values. Such increases could have serious implications for flooding.

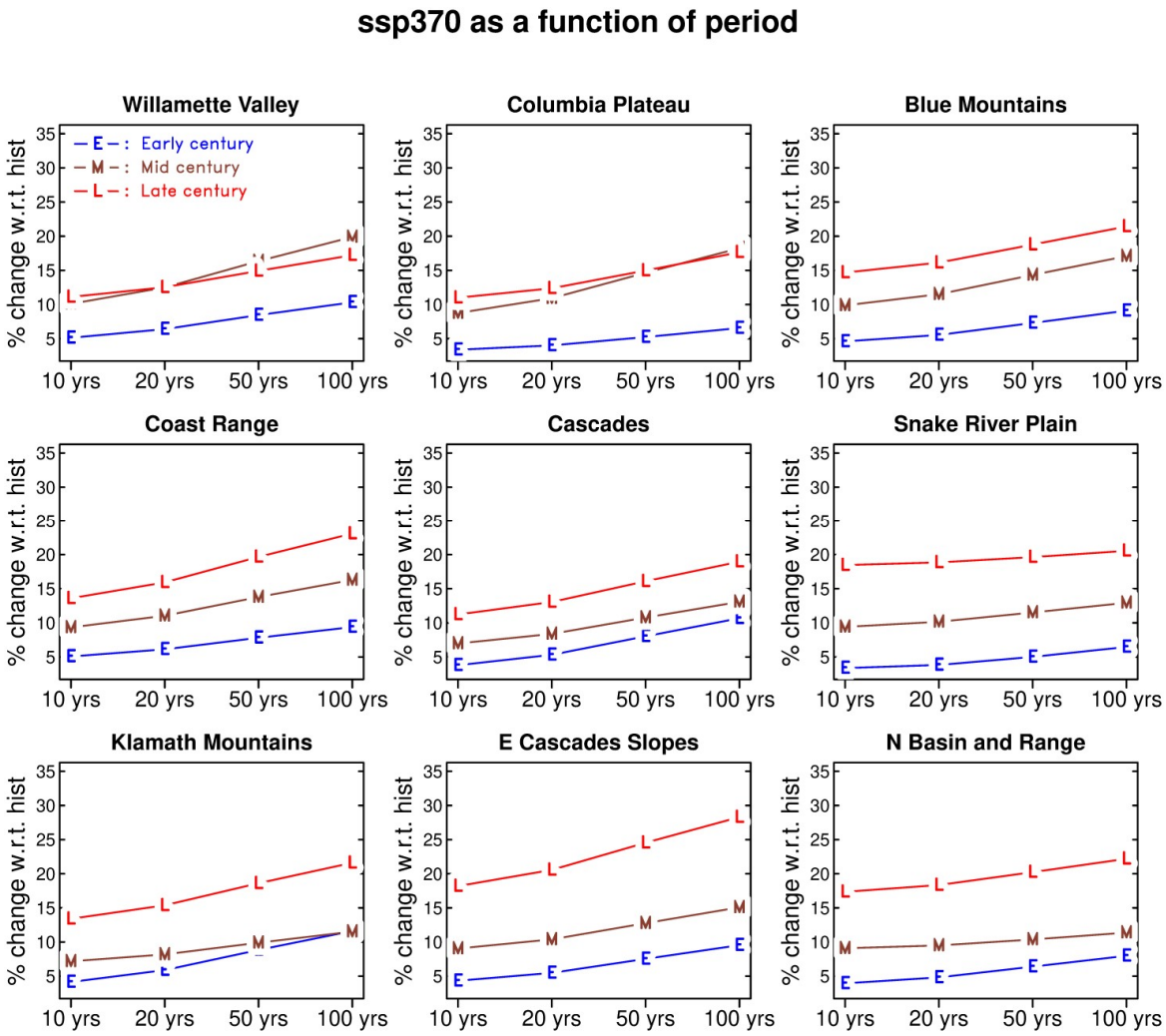

Figure 13. Multi-model ensemble average projected changes (%) in return values of wet-day precipitation by early century (2014-2044, blue line with "E"), midcentury (2045-2074, brown line with "M") and late century (2075-2100, red line with "L"). Changes are calculated with respect to the historical period, for the SSP 3-7.0 emissions scenario. Panels are arranged roughly geographically in the state.

Snow to rain transition

A critical aspect of precipitation for water management and natural systems is how much precipitation falls as rain vs. snow, since snow retains winter precipitation and releases it slowly over the course of spring to early summer. Lack of winter snow increases the likelihood of hydrological or agricultural drought during the following spring and summer.

In water management applications a key aspect of snow is not how deep it is, but how much water it contains. This is termed the snow water equivalent (SWE) of the snow. For example, 10 cm of snow might contain 1 cm of water when melted, in which case the SWE of the snow is 1 cm. The ratio of the depth of the snow to the SWE of the snow depends on numerous factors, including the characteristics of the storm that dropped the snow, the temperature at which the snow formed, the

temperature history of the snowpack, the heat flux from the ground to the snowpack, and the age of the snowpack.

We use an analogous concept here when we discuss precipitation in the form of snow. Rather than considering the depth of the snow that accumulates on the ground, we consider the snow water content of the snow that falls, which we label as SWE snowfall. For example, if 10 cm of snow falls in a day and that snow contains 1 cm of water, we say that there is 1 cm of SWE snowfall. This approach is useful both because the water content of snow is of key importance for water management purposes and because the underlying data used here consists of total precipitation measured by water content and does not have information on snow depth.

We estimate SWE snowfall rate (mm/day) from daily minimum (Tmin), maximum (Tmax), and average (Tavg = 0.5*(Tmin + Tmax)) temperatures and total precipitation (P, mm/day) using the algorithm shown in Figure 14. The SWE snowfall algorithm employed here is based on that used in the Variable Infiltration Capacity (VIC) hydrological model (Liang et al., 1994) and MTCLIM meteorological estimation model (Hungerford et al., 1989), which determine whether total precipitation supplied to the VIC model is to be interpreted as rain or snow.

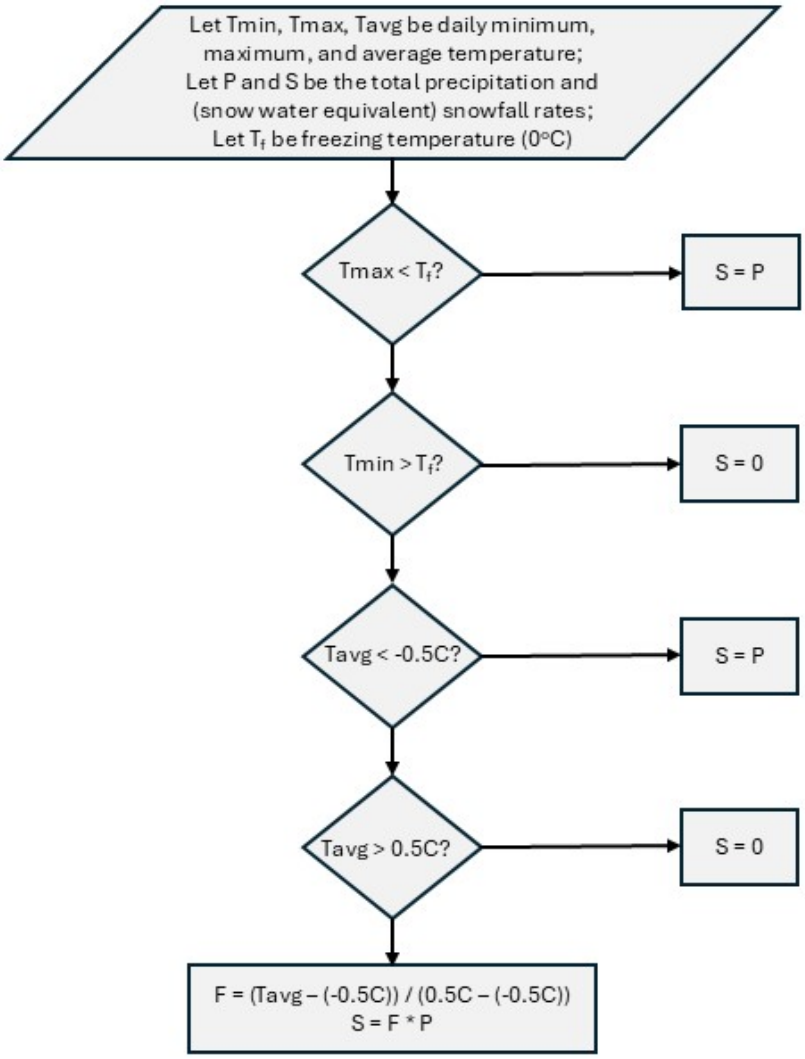

Figure 14. Process for determining the snow water equivalent (SWE) snowfall rate, S, from daily temperature (Tmin, Tmax, Tavg) and precipitation rate (P).

The historical seasonal mean total precipitation, rainfall, and SWE snowfall are shown in Figure 15, although summer is omitted in this entire section because of the very low values of SWE snow in that season. Unsurprisingly, snowfall peaks in winter, with the largest Oregon values seen in the Cascades during winter. Snowfall in the Cascades is prevalent in spring and autumn as well.

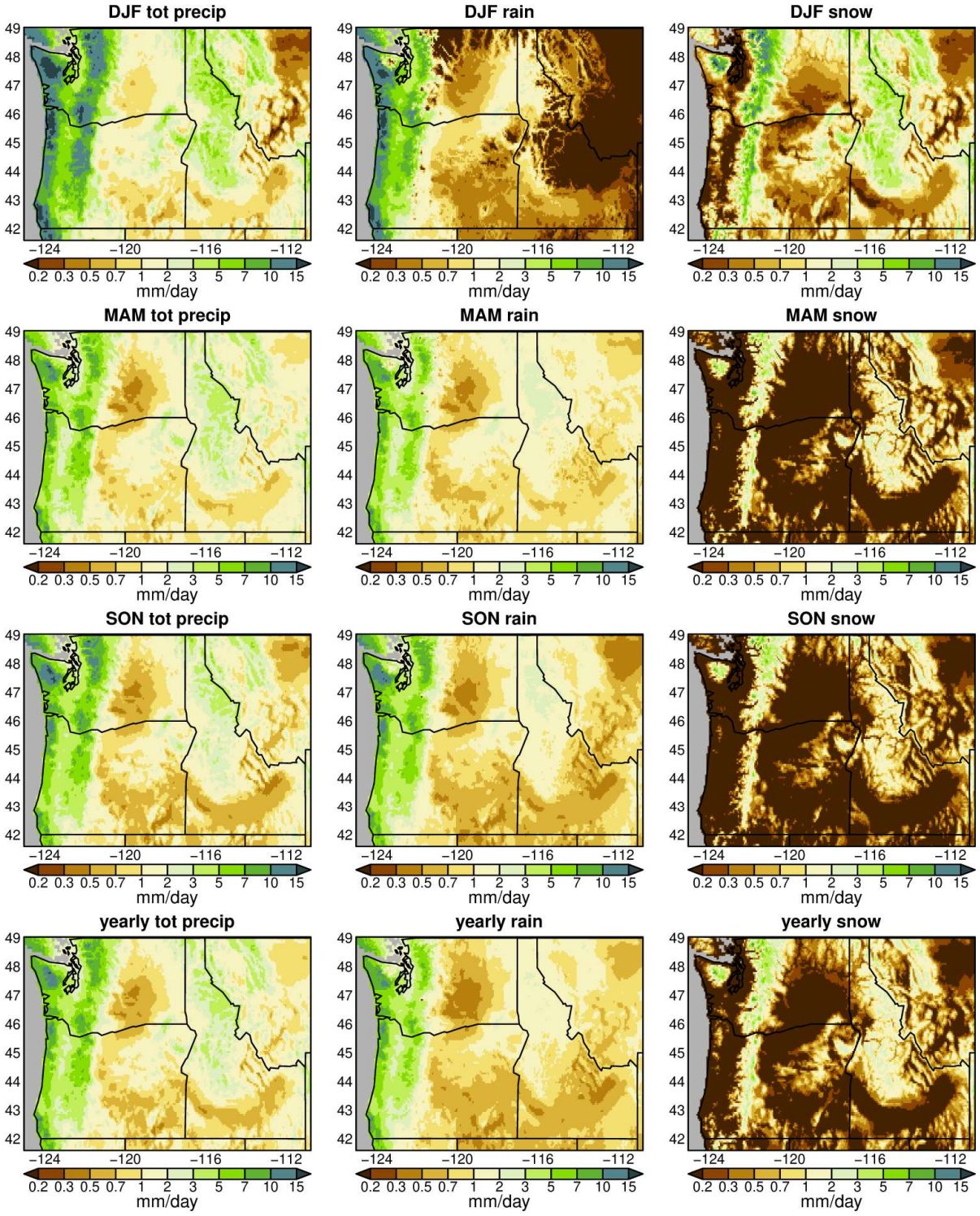

Figure 15. For the historical period, multi-model ensemble average total precipitation (i.e., rain + snow; left column), precipitation that falls as rain (middle column), and precipitation that falls as snow (right column), in mm/day of snow water equivalent. Results are shown for winter (top row), spring (second row), autumn (third row), and yearly (bottom row). Summer is omitted due to very little snow falling during that season.

The rain/snow split, illustrated as the percent of total precipitation that falls as SWE snow, is shown in Figure 16 for the historical period and midcentury (2044-2074) using the SSP 3-7.0 emissions scenario. The coastal regions of the Pacific Northwest have low SWE snowfall fractions even in winter, with values typically less than 10%. Interior Idaho, by contrast, is characterized by SWE snowfall fractions over 95% in winter. The highest SWE snowfall fractions in Oregon are seen in the Cascades and Blue Mountains, where winter SWE snowfall fractions can exceed 50%. By midcentury, large swaths of the state experience decreases in SWE snowfall fraction of 10-25 percentage points in winter (right column of Figure 16), and 5-20 percentage points annually. The main exception to this is the coastal regions, which have low SWE snowfall fractions to begin with and so are not able to decrease appreciably in percentage points.

The spread across all 11 models of future projected winter (DJF) SWE snowfall percentage changes is shown, by region, in Figure 17 for the SSP 3-7.0 emissions scenario. One of the models, TaiESM1, shows a notably higher future SWE snowfall fraction in the Willamette Valley and Coast Range than seen in any other model. However, these are the regions where the historical SWE snowfall fraction is low (Figure 16), so small absolute changes can equate to large percentage changes in those regions. In the other regions the spread across models is smaller but still illustrates how the models have a spectrum of projected responses in the future. The chaotic nature of weather means that even a perfect model of the Earth would have a spread of future climate changes; climate is probabilistic, not deterministic. For example, consider the projected midcentury (2045-2074) SWE snowfall fraction changes in the Cascades ecoregion (center panel of Figure 17). Keeping in mind that these are estimates due to having only 11 models, these results suggest that the midcentury reduction in SWE snowfall fraction due to anthropogenic forcing is about 45% (the value of the multi-model ensemble average line), and natural climate variability can alter this by about +/- 10 percentage points (the spread of the models around the multi-model ensemble average line).

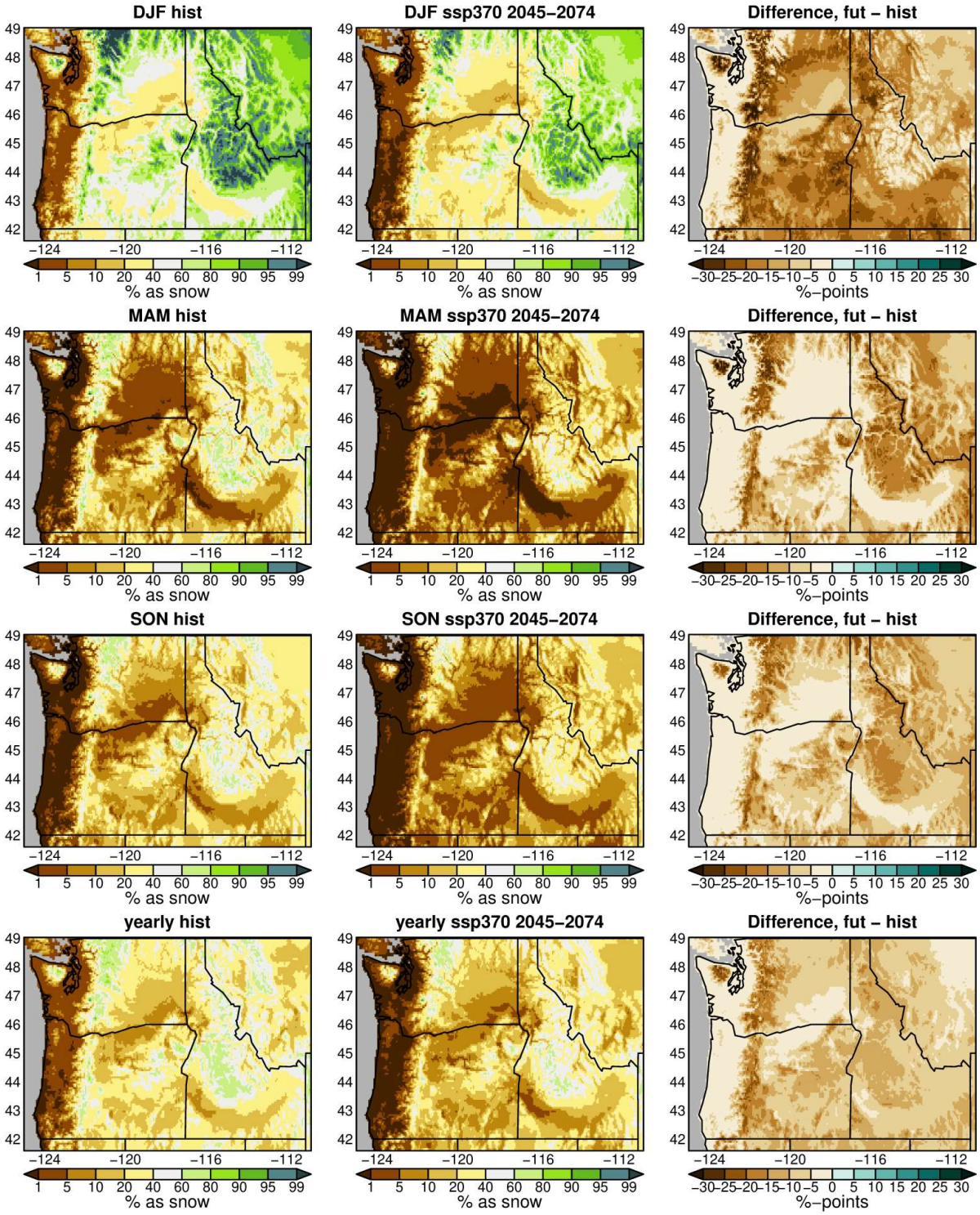

Figure 16. Left column: multi-model ensemble average historical SWE snowfall fraction (i.e., percent of total precipitation that falls as SWE snow). Middle: midcentury (2045-2074) snow fraction under the SSP 3-7.0 emissions scenario. Right: difference between midcentury and historical snow fraction, in percentage points (midcentury value minus historical value).

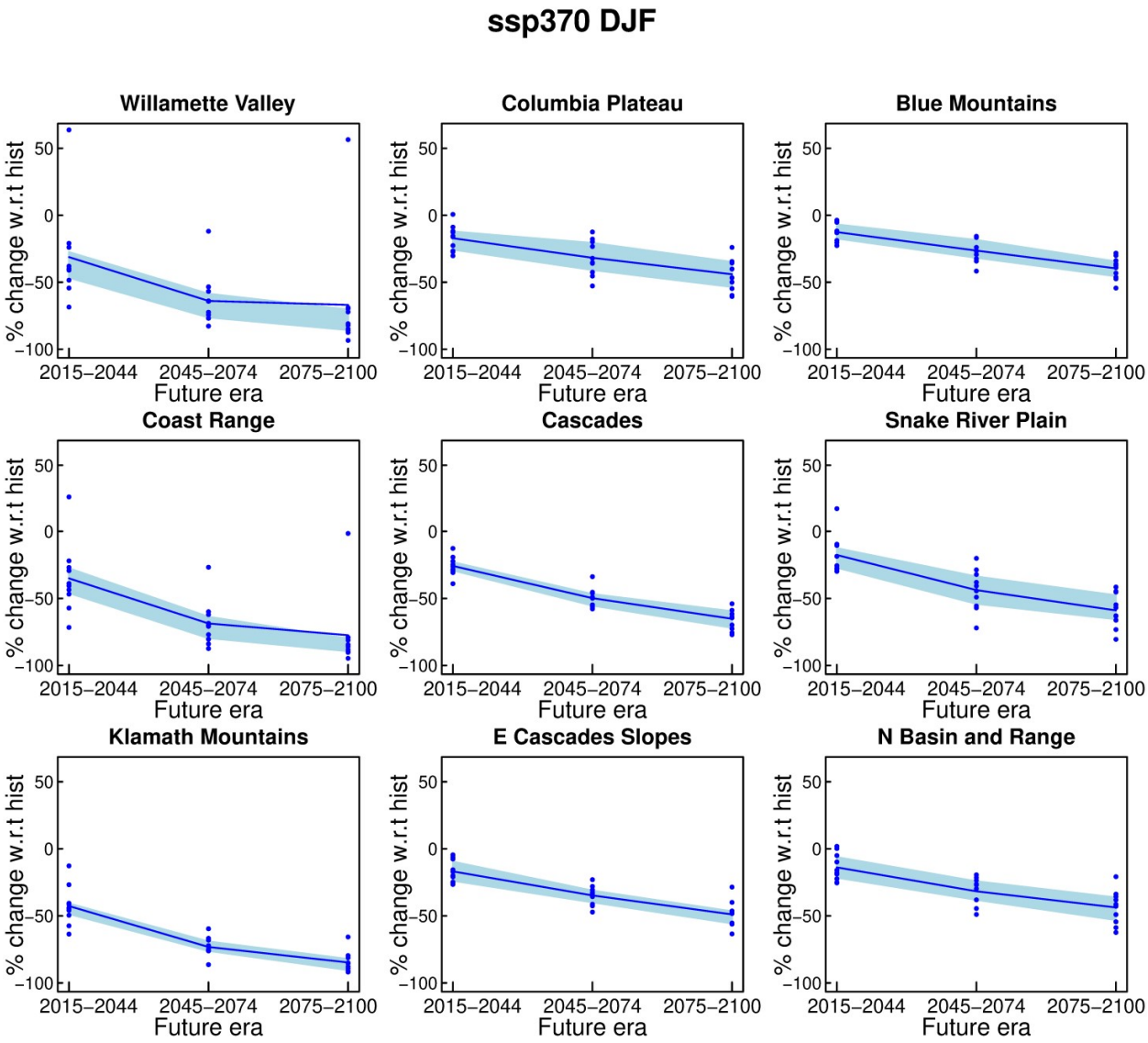

Figure 17. Projected change in SWE snowfall fraction (%), by region, as a function of time for the SSP 3-7.0 emissions scenario. The blue line is the multi-model ensemble average. The light blue envelope shows the interquartile range (IQR) across all 11 available models. Blue dots show each individual model.

Augmenting the SWE snow fraction change maps, Figure 18 shows SSP 3-7.0 projected midcentury changes in both absolute (mm/day; middle column) and relative (%; right hand column) SWE snowfall. The largest absolute changes are seen in winter in the Cascades, where decreases of 2-3 mm/day SWE are common. These represent relative decreases of 20-60% (right column).

The largest relative changes in SWE snowfall are seen in spring, with widespread decreases exceeding 80% in western Oregon, although it should be noted that there is only minor snowfall in this region and season to begin with (left column). Autumn has results similar to spring. Midcentury changes in winter SWE snowfall are negative in most but not all areas, commonly amounting to declines of 40% or more. Exceptions to this pattern of diminished winter SWE snowfall are incremental gains in parts of the northern Cascades and portions of the Rocky Mountains in Idaho and Montana.

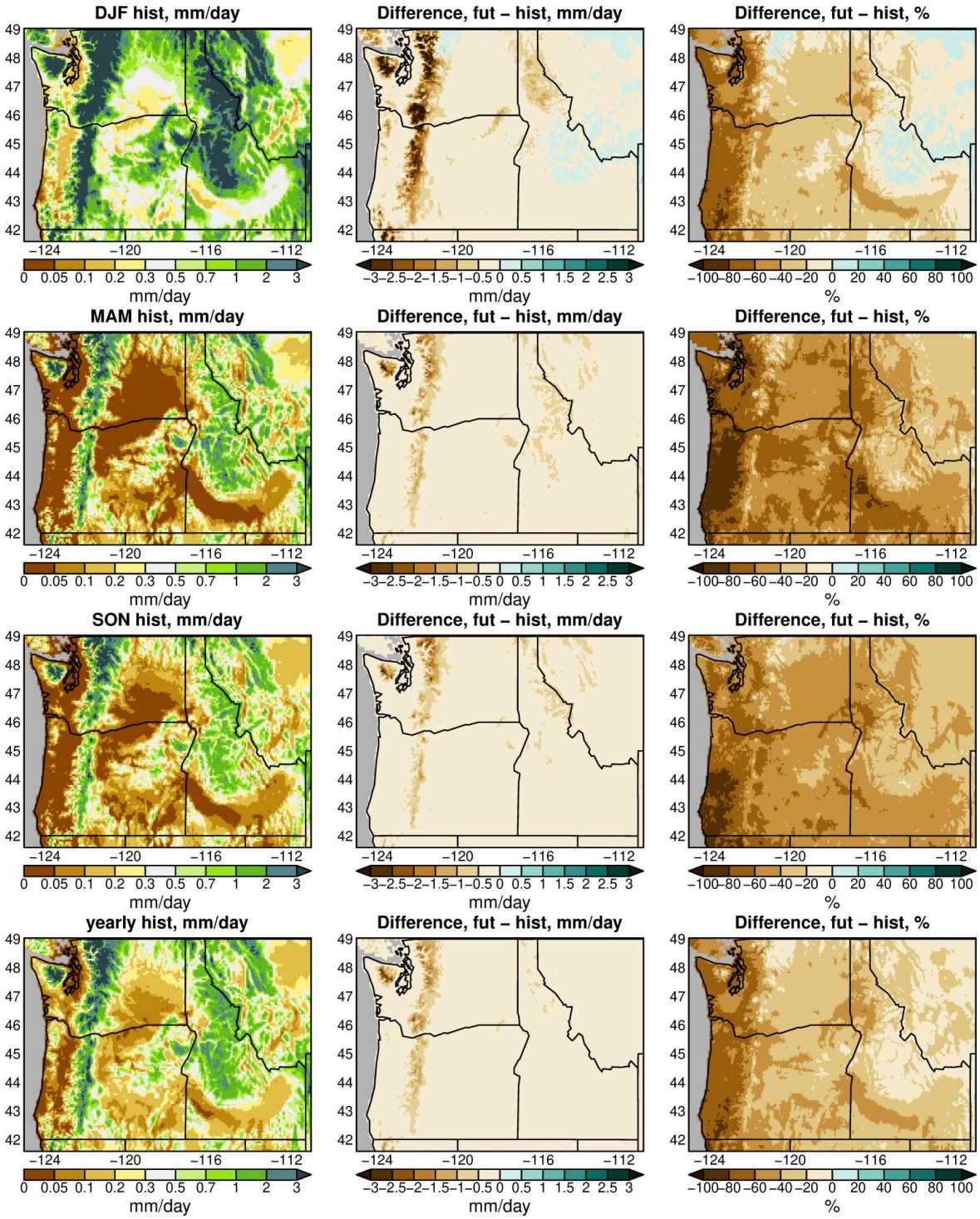

Figure 18. Left column: multi-model ensemble average historical SWE snowfall (mm/day), by season (omitting summer) and yearly. Middle column: multi-model ensemble average projected change in SWE snowfall for the midcentury (2045-2074) relative to historical SWE snowfall in mm/day. Right column: projected changes in percent.

Complementary to the wholesale reductions in future snowfall are increases in rainfall, illustrated in Figure 19 for the midcentury (2045-2074) using the SSP 3-7.0 scenario. As in Figure 18, the left column shows historical values in mm/day, the center column shows multi-model ensemble average projected changes in mm/day, and the right column shows multi-model ensemble average projected changes in percent.

Largely reflecting the loss of SWE snowfall, the largest absolute (mm/day) rainfall increases are found in winter, particularly in the Cascades and Olympic peninsula, where relative (percent) changes can reach over 400% in Washington state and 200% in the state of Oregon in the Cascades and Blue Mountains. Notable changes are seen in spring, autumn, and yearly as well. In the yearly total, much of the Cascades and eastern Oregon show projected rainfall increases between 10% and 50%, which could have substantial impact on ecosystems and flooding in the region.

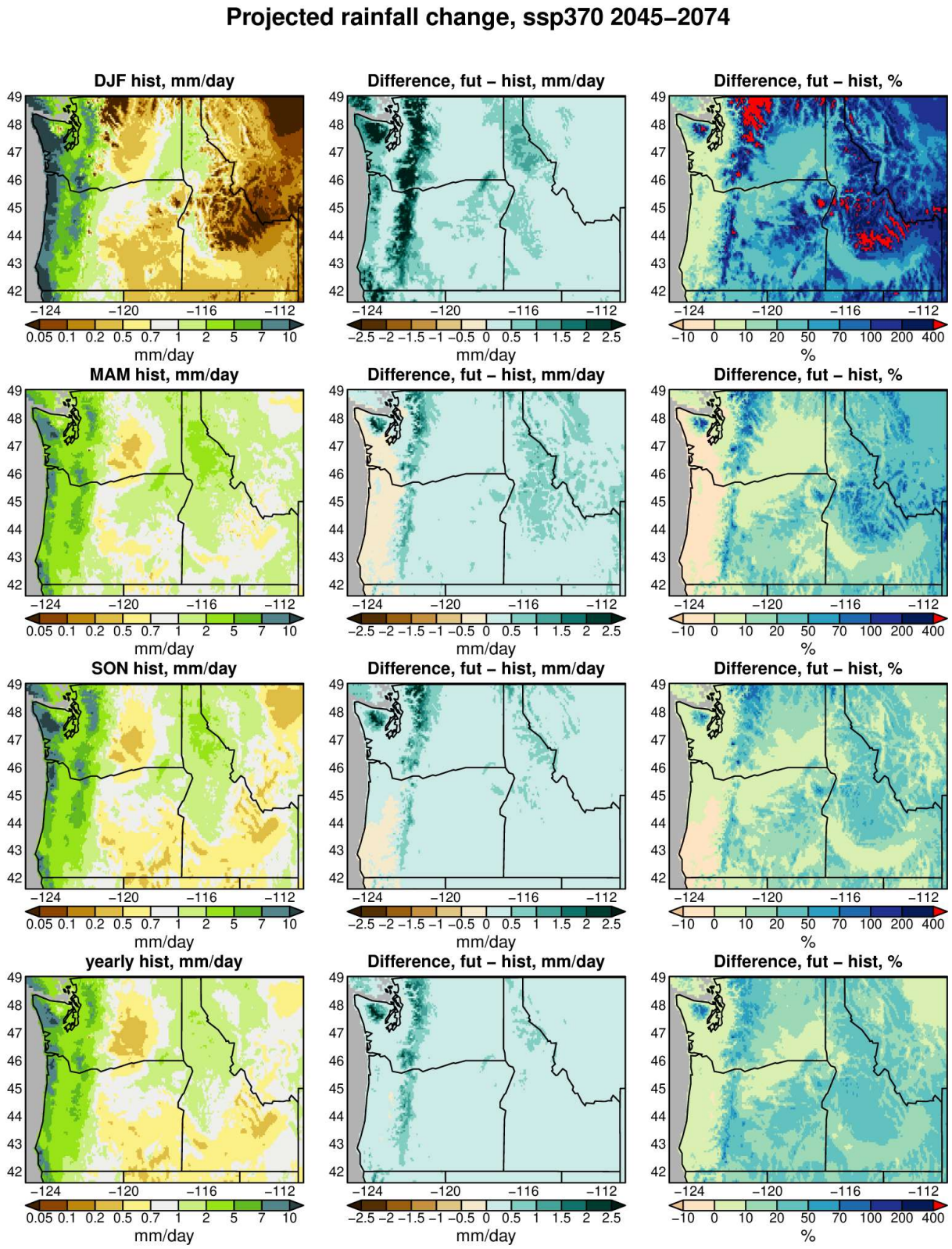

Figure 19. Left column: multi-model ensemble average historical rainfall (mm/day). Middle: multi-model ensemble average projected changes in rainfall for the midcentury (2045-2074) under the SSP 3-7.0 emissions scenario, in mm/day. Right column: projected change in percent.

Figure 13 shows that the magnitude of future extreme precipitation events is projected to increase throughout Oregon, with most locations exhibiting growing increases as the 21st century progresses. At the same time Figure 19 shows the decided transition from snow to rain in much of the state. This leads to the question of whether extreme rainfall events will increase at a greater rate than extreme total precipitation rates, since both the increasing magnitude of precipitation events and the conversion from snow to rain are at play. This is examined in Figure 20, which compares the midcentury projected change in extreme return values of total precipitation from Figure 13 to the same quantity calculated for rainfall alone.

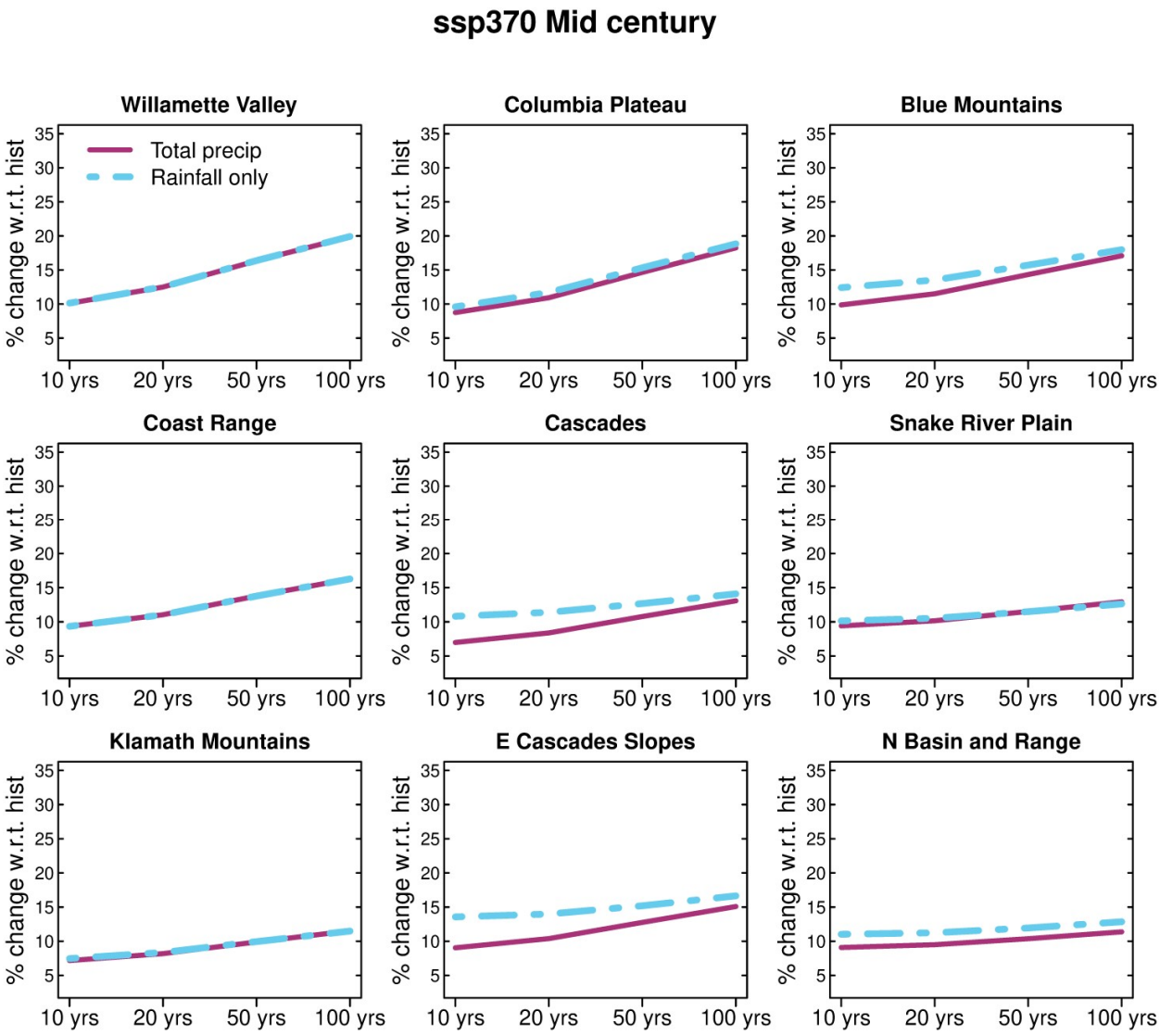

Figure 20. Multi-model ensemble average projected changes (%) in return values of wet-day precipitation by midcentury (2045-2074, purple solid line), and changes in rainfall alone in the same period (dashed blue line). Changes are calculated with respect to the historical period, for the SSP 3-7.0 emissions scenario.

Little difference between return values of total precipitation (rain + snow) and rainfall alone are seen in the western/coastal part of the state, in accord with Figure 16, which shows that SWE snow fraction is low in those regions. The largest rainfall increases are seen in the Cascades and Eastern

Cascades Slopes, where the conversion from snow to rain is both an appreciable fraction of total precipitation (Figure 16, right hand column) and has appreciable absolute magnitudes (in mm/day, Figure 18, center column). In these regions the 10-yr return value of rainfall increases notably more than the corresponding return value of total precipitation (11% rain vs. 7% total precipitation for the Cascades, and 14% vs. 9% for the Eastern Cascades Slopes). Smaller increases in rain relative to total precipitation are seen in the Blue Mountains and North Basin and Range. Interestingly, the projected future increases at the most extreme return periods considered here, 100 years, are only marginally different between rainfall and total precipitation. This suggests that some of the biggest storms, as measured by production of precipitation, have historically produced snow, and that these large storms will tend to continue to be cold enough to produce snow by midcentury.

A concise way of representing the changes in rainfall, SWE snowfall, and total precipitation (rain+snow) by region over the full time extent of the data is shown in Figure 21. The indicated changes in percent are calculated as the change from 1950-1959, the first decade of data, to 2091-2100, the last decade of data. Although we primarily focus on changes by mid 21st century (2045-2074) in this work, it is worth keeping in mind that longer time period changes are important as well, especially to ecosystems, existing built infrastructure, and long-lived residents of the state.

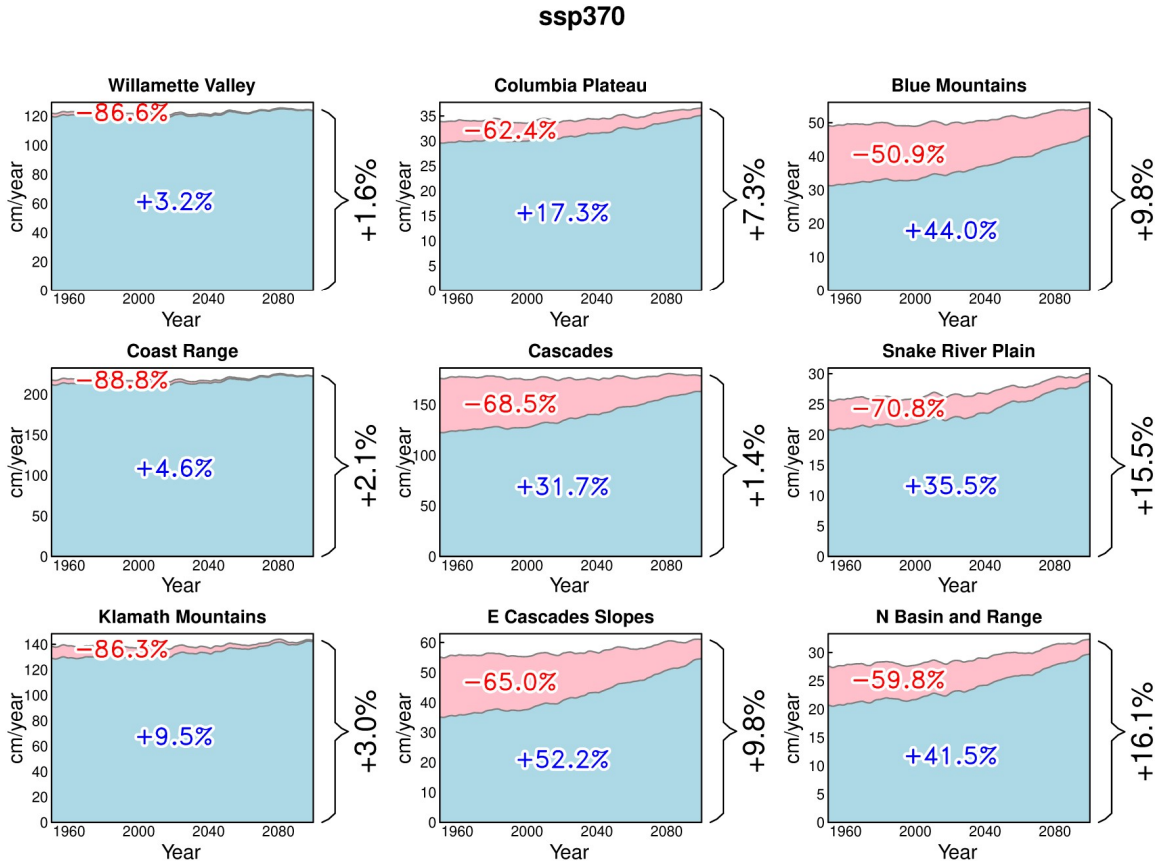

Figure 21. Multi-model ensemble average SSP 3-7.0 projected regional annual total rainfall (blue), SWE snowfall (pink), and total precipitation (rain + SWE snowfall; black) over the entire data period of 1950 to 2100. Changes from the first (1950-1959) to the last (2091-2100) decade of the record are shown in percent. To reduce natural internal variability and clarify the underlying trends, a third order Butterworth low-pass filter with cutoff of 0.1 cycles/yr has been applied to the time series.

SWE snowfall declines strongly in the state over this time period, with all regions losing at least half their SWE snowfall. By the measure of changes in the snow/rain split, the Cascades and Eastern Cascades Slopes are the regions most strongly affected by anthropogenic climate change on the longer time scales. Over the entire data period (from the decade of the 1950's to the decade of the 2090's) 68% of SWE snowfall is projected to be lost in the Cascades and 65% in the Eastern Cascade slopes, under the SSP 3-7.0 emissions scenario. Increases in rainfall are also large in many regions, with increases of 30-50% over much of the southeastern part of the state. Although the regions near the coast (Coastal Range, Willamette Vally, and Klamath Mountains) are projected to experience the largest percentage loss of SWE snowfall, the actual values of snowfall there are low compared to the Cascades. Because of this, the loss of SWE snowfall does not give rise to appreciable increases in yearly averaged rainfall.

Uncertainty and variability

Stakeholders may understand that climate projections contain uncertainty and variability but may not entirely understand the sources. Three main factors contribute to this uncertainty: 1) What humans choose to do in the future, and in particular, the quantity of greenhouse gases that will be emitted in the future due to human activity. This is referred to as scenario uncertainty. 2) How climate models differ in depicting the physical processes that produce the climate, which is referred to as model uncertainty. 3) Natural climate and weather variability, for example, the path of a particular storm, occurrence of a dry summer in the Pacific Northwest region, or phase of the El Niño-Southern Oscillation. This is referred to as uncertainty due to internal climate variability.

Hawkins and Sutton (2009) first showed that the leading source of climate projection uncertainty on the global scale depends on the model projection (forecast) lead time. By the end of the 21st century, overall uncertainty in global climate change is largely determined by scenario uncertainty, which is to say, what humans choose to do (if anything) in response to the issue of climate change. The climate effect of greenhouse gas emissions is so large that the amount of greenhouse gases emitted swamps uncertainty from models and internal variability. In this sense humanity is free to choose its own climate future.

At lead times of about 15-45 years from present, uncertainty is primarily due to model disagreements, i.e., different depictions of climate processes in different global climate models. This is one of the motivations for selecting models that do a good job simulating climate in the region of interest when concentrating on midcentury climate projections, as is done in this work. Scenario uncertainty is less than model uncertainty at these intermediate lead times partly because the emissions scenarios diverge most strongly from each other after the middle of the 21st century. Model uncertainty continues to be the second largest part of overall global climate change uncertainty out to the end of the century, highlighting the importance of continuing to improve the quality of climate models.

Internal climate variability, including the initial state of the Earth's climate system and the detailed evolution of weather events and natural climate fluctuations, is the dominant factor in climate projection uncertainty on lead times of 0 to 15 years. Climate projections on these relatively shorter timescales are sometimes referred to as decadal climate forecasts, and have attracted significant scientific interest due to the utility that a decadal climate forecast could provide.

Moving from the global to more regional (Pacific Northwest) or state (Oregon) spatial scales, other considerations come into play in scoping possible climate outcomes, particularly when looking at precipitation extremes. By definition, extremes are a rare occurrence, so there is considerable sampling uncertainty in estimating the true return value given a limited data record. Furthermore, any one particular 10-year period is unlikely to experience exactly the 10-year return value extreme precipitation event; what actually happens in a single decade could be larger or smaller than what is expected based on the long-term statistics. Natural variability also means that a storm that generates extreme precipitation could devastate one particular town but largely miss a nearby town, so there can be large spatial variation in the occurrence of extremes. Even within cities, topographic features such as hills can cause local microclimates that experience different precipitation extremes from the same storm.

Given these various sources of uncertainty in the climate projections, practitioners should keep in mind that systematic changes from greenhouse gas emissions, aerosols, land use changes, and other factors will have a discernible effect on future climate, as shown in this work. The actual future experienced at any particular location will be a combination of the changes that arise from human-caused climate change and from random, unpredictable fluctuations that arise from natural climate variability. Although natural climate variability has been a part of planning processes for decades and many planning processes already incorporate this kind of uncertainty, results such as found here demonstrate that likely changes that arise from human-caused climate change need to be added to the planning process when considering future climate conditions in the state. Merely assuming that past climate conditions will continue into the future unchanged is not supported by the evidence and could lead to significant risks.

Summary

In this work we have examined the projected future changes in precipitation and rain/snow partition in Oregon and adjacent northwestern states that arise from anthropogenic climate change. Eleven global climate models were selected for analysis based on their ability to realistically simulate key weather processes and historically observed climatology and variability over the region of interest. Statistically downscaled and bias corrected data were then used to examine model-projected future changes in precipitation, focusing on extreme precipitation events and the rain/snow split. The period of data is 1950-2100, but we focus on model-projected changes by midcentury (2045-2074) as the period most relevant for typical planning purposes. Three greenhouse gas and aerosol emissions scenarios were considered, with the results presented here focusing on the middle emissions scenario, SSP 3-7.0.

Models show a weak tendency towards higher precipitation (0-10%) in the state overall by midcentury, but with seasonal variation that includes drier summer conditions in western Oregon (by 5-15%). This could affect the incidence of wildfires in the region. Extreme wet-day precipitation increases progressively as the century advances, with domain-average projected increases of about 7% by midcentury in the SSP 3-7.0 scenario for the 99th percentile wet day. In Oregon, these changes are largest in winter, particularly in the southeastern portion of the state, and continue to increase towards the end of the century. In the western part of the state and heavily populated

Willamette Valley, the largest projected increases in extreme daily precipitation are seen in autumn, with values approaching 10% for the 99th percentile and 20% for the 99.9th percentile by midcentury.

The fraction of annual total precipitation that falls as snow is projected to decrease by midcentury by 10-20% over much of Oregon from the Cascades ecoregion to the east, with the largest decreases in spring, where reductions across much of the state reach 40-80%. As a result rainfall is projected to increase by midcentury, with annually averaged increases of 10-20% over much of the state from the Cascades eastwards, as snowfall converts to rainfall.

Over the full span of data available for analysis (1950-2100), SWE snowfall is projected to decrease by at least 50% in every part of the state, with decreases of over 65% in the Cascades and over 85% in the western portion of the state. Precipitation falling as rain correspondingly increases, by 30-50% over much of the southeastern portion of the state, but only 3-10% of the western and coastal areas due to less snowfall there to begin with. Such changes could have important impacts on existing water management and flood protection infrastructure.

Acknowledgements

This work was made possible by funding from the Oregon Climate Change Research Institute at the Oregon State University, by the SERDP program sponsored by the U.S. Department of Defense, and by funding from the California Energy Commission. This support is gratefully acknowledged.

We acknowledge the World Climate Research Programme, which, through its Working Group on Coupled Modelling, coordinated and promoted CMIP6. We thank the climate modeling groups for producing and making available their model output, the Earth System Grid Federation (ESGF) for archiving the data and providing access, and the multiple funding agencies who support CMIP6 and ESGF.

References

Arrhenius, S., 1896: On the influence of carbonic acid in the air upon the temperature of the ground. The London, Edinburgh, and Dublin Philosophical Magazine and J. Science, v. 41, p. 8.

Eyring, V., S. Bony, G. A. Meehl, C. A. Senior, B. Stevens, R. J. Stouffer, and K. E. Taylor, 2016: Overview of the Coupled Model Intercomparison Project Phase 6 (CMIP6) Experimental Design and Organization. *Geosci. Mod. Devel.*, **9**, 1937-1958, doi:10.5194/gmd-9-1937-2016.

Harp, R. D.,and Horton, D. E., 2022: Observed changes in daily precipitation intensity in the United States. *Geophys. Res. Lett.,* **49**, e2022GL099955. https://doi.org/10.1029/2022GL099955

Hawkins, E., and R. Sutton, 2009: The potential to narrow uncertainty in regional climate predictions. *Bull. Am. Met. Soc.*, Aug. 2009, p. 1095, DOI: 10.1175/2009BAMS2607.1.

Hosking, J. R., 1990: L-moment - Analysis and Estimation of Distributions Using Linear-combinations of Order-statistics. *J. Royal Statistical Society Series B-methodological*, 52, 105-124

Hungerford, R. D., R. R. Nemani, S. W. Running, and J. C. Coughlan, 1989: MTCLIM: A mountain microclimate simulation model. Res. Pap. INT-RP-414. Ogden, UT: U.S. Department of Agriculture, Forest Service, Intermountain Research Station. 52 p. https://doi.org/10.2737/INT-RP-414

IPCC, 2023: *Climate Change 2023: Synthesis Report.* Contribution of Working Groups I, II and III to the Sixth Assessment Report of the Intergovernmental Panel on Climate Change [Core Writing Team, H. Lee and J. Romero (eds.)]. IPCC, Geneva, Switzerland, pp. 35-115, doi: 10.59327/IPCC/AR6-9789291691647.

Krantz, W., D. W. Pierce, N. Goldenson, and D. R. Cayan, 2021: Memorandum on evaluating global climate models for studying regional climate change in California. Technical report for California Energy Commission project EPC-20-006, 24 pp., available at https://www.energy.ca.gov/sites/default/files/2022-09/20220907_CDAWG_MemoEvaluating_GCMs_EPC-20-006_Nov2021-ADA.pdf

Kroner, N., S. Kotlarski, E. Fischer, D. Luthi, E. Zubler, and C. Schar, 2017: Separating climate change signals into thermodynamic, lapse-rate and circulation effects: theory and application to the European summer climate. *Clim. Dyn.*, **48**, 3425-3440, doi:10.1007/s00382-016-3276-3.

Liang, X., D. P. Lettenmaier, E. F. Wood, and S. J. Burges, 1994: a Simple Hydrologically Based Model of Land-surface Water and Energy Fluxes for General-circulation Models. *J. Geophys. Res.-atmospheres*, **99**, 14415-14428, doi:10.1029/94JD00483.

Lybarger, N. D., A. Smith, A. J. Newman, E. D. Gutmann, A. W. Wood, C. D. Frans, M. D. Warner, and J. R. Arnold, 2024: Improving Earth System Model selection methodologies for projecting hydroclimatic change: Case study in the Pacific Northwest. J. Geophys. Res. Atmos., e2023JD039774, https://doi.org/10.1029/2023JD039774.

Norris, J., G. Chen, and J. D. Neelin, 2019: Thermodynamic versus Dynamic Controls on Extreme Precipitation in a Warming Climate from the Community Earth System Model Large Ensemble. *J. Clim.*, **32**, 1025-1045, doi:10.1175/JCLI-D-18-0302.1.

O'Neill, B .C., E. Kriegler, K. Riahi et al., 2014: A new scenario framework for climate change research: the concept of shared socioeconomic pathways, *Climatic Change*, **122**, 387, doi:10.1007/s10584-013-0905-2.

O'Neill, B. C., et al. 2016: The Scenario Model Intercomparison Project (ScenarioMIP) for CMIP6, *Geosci. Model Dev.*, **9**, 3461–3482, doi:10.5194/gmd-9-3461-2016.

Pierce, D. W., T. P. Barnett, B. D. Santer, and P. J. Gleckler, 2009: Selecting Global Climate Models for Regional Climate Change Studies. *Proc. Nat. Acad. Sci.*, **106**, 8441-8446, doi:10.1073/pnas.0900094106.

Pierce, D. W., D. R. Cayan, and B. L. Thrasher, 2014: Statistical Downscaling Using Localized Constructed Analogs (LOCA). *J. Hydromet.*, **15**, 2558-2585, doi:10.1175/JHM-D-14-0082.1.

Pierce, D. W., D. R. Cayan, E. P. Maurer, J. T. Abatzoglou, and K. C. Hegewisch, 2015: Improved Bias Correction Techniques for Hydrological Simulations of Climate Change. *J. Hydromet*., **16**, 2421-2442, doi:10.1175/JHM-D-14-0236.1.

Pierce, D. W., L. Su, D. R. Cayan, M. D. Risser, B. Livneh, and D. P. Lettenmaier, 2021: An Extreme-Preserving Long-Term Gridded Daily Precipitation Dataset for the Conterminous United States. *Journal of Hydrometeorology*, v. 22, p. 1883-1895. https://doi.org/10.1175/JHM-D-20-0212.1

Pierce, D. W., D. R. Cayan, D. R. Feldman, and M. D. Risser, 2023: Future increases in North American extreme precipitation in CMIP6 downscaled with LOCA. *J. Hydrometeorology*. DOI: 10.1175/JHM-D-22-0194.1

Riahi, K., D. P. van Vuuren, E. Kriegler, J. Edmonds, B. C. O'Neill, S. Fujimori, N. Bauer, K. Calvin, R. Dellink, et al., 2017: The Shared Socioeconomic Pathways and Their Energy, Land Use, and Greenhouse gas Emissions Implications: An Overview. *Glob. Environ. Chg.-human And Policy Dimensions*, **42**, 153-168, doi:10.1016/j.gloenvcha.2016.05.009.

Westra, S., H. J. Fowler, J. P. Evans, L. V. Alexander, P. Berg, F. Johnson, E. J. Kendon, G. Lenderink, and N. M. Roberts, 2014: Future changes to the intensity and frequency of short-duration extreme rainfall. *Rev. Geophys*., **52**, 522-555, doi:10.1002/2014RG000464.